NASA CONTRACTOR REPORT

NASA CR-2768

NASA CR-2768

FLOAT-ZONE PROCESSING IN A WEIGHTLESS ENVIRONMENT

A. A. Fowle, J. S. Haggerty, R. R. Perron, P. F. Strong, and J. L. Swanson

Prepared by
ARTHUR D. LITTLE, INC.
Cambridge, Mass.
for George C. Marshall Space Flight Center

NATIONAL AERONAUTICS AND SPACE ADMINISTRATION • WASHINGTON, D. C. • NOVEMBER 1976

1. REPORT NO.	2. GOVERNMENT ACCESSION NO.	3. RECIPIENT'S CATALOG NO.
NASA CR-2768		

4 TITLE AND SUBTITLE	5. REPORT DATE
Float-Zone Processing in a Weightless Environment	November 1976
	6. PERFORMING ORGANIZATION CODE

7. AUTHOR(S)	8. PERFORMING ORGANIZATION REPORT #
A. A. Fowle, J. S. Haggerty, R. R. Perron, P. F. Strong, and J. L. Swanson	M-190

9. PERFORMING ORGANIZATION NAME AND ADDRESS	10. WORK UNIT NO.
Arthur D. Little, Inc. Cambridge, Massachusetts	11. CONTRACT OR GRANT NO. NAS8-29877
	13. TYPE OF REPORT & PERIOD COVERED
12. SPONSORING AGENCY NAME AND ADDRESS	Contractor
National Aeronautics and Space Administration Washington, D. C. 20546	14. SPONSORING AGENCY CODE

15. SUPPLEMENTARY NOTES

16. ABSTRACT

This report documents the results of investigations to: 1) test the validity of previous analyses which set maximum practical diameters for Si crystals that can be processed by the float zone method in a near weightless environment, 2) determine the convective flow patterns induced in a typical float-zone, Si melt under conditions perceived to be advantageous to the crystal growth process using flow visualization techniques applied to a dimensionally scaled model of the Si melt, 3) revise the estimates of the economic impact of space-produced Si crystal by the float-zone method on the U. S. electronics industry, and 4) devise a rational plan for future work related to crystal growth phenomena wherein low-gravity conditions available in a space site can be used to maximum benefit to the U. S. electronics industry.

17. KEY WORDS	18. DISTRIBUTION STATEMENT
	STAR Category 88

19. SECURITY CLASSIF. (of this report)	20. SECURITY CLASSIF. (of this page)	21. NO. OF PAGES	22. PRICE
Unclassified	Unclassified	82	$4.75

* For sale by the National Technical Information Service, Springfield, Virginia 22161

FOREWORD

This report documents the results of investigations to: 1) test the validity of previous analyses (reported in Interim Report, "Float Zone Processing in a Weightless Environment", Contract NAS8-29877, October 1974) which set maximum practical diameters for Si crystals that can be processed by the float zone method in a near weightless environment, 2) determine the convective flow patterns induced in a typical float-zone, Si melt under conditions perceived to be advantageous to the crystal growth process using flow visualization techniques applied to a dimensionally scaled model of the Si melt, 3) revise the estimates of the economic impact of space-produced Si crystal by the float-zone method on the U.S. electronics industry, and 4) devise a rational plan for future work related to crystal growth phenomena wherein low gravity conditions available in a space site can be used to maximum benefit to the U. S. electronics industry.

Experimental confirmation of the theoretically predicted,* (1) least stable limit of operation under conditions of co-axial rotation of the polycrystalline feed stock and growing crystal having equal diameters has been made. Considering other important determinants of the crystal growth process, this stability limit has small impact on the potentially practical size or perfection of crystal to be grown in space.

Observations of the flow induced within the model melt by equal counter rotation have determined that for low rotational rates (at Reynolds' numbers, based on the peripheral speed of the model crystal or feed stock, of less than 60), the flow streamlines have a continuous helix-within-a-helix character, with the number of coils dependent on the rotation rate. A unique, flat plane of symmetry exists which separates mirror-image streamlines patterns in the upper and lower counter-rotating cells. At intermediate rotational rates (Reynolds' numbers near 150) several unexpected surface swirls were observed precessing about the circumference of the float-zone model. The relationship of this phenomenon to the core flow, and the impact on float-zone crystal growth need to be resolved. Limitations in tracer particle reflectivity prevented photography at high rotation rates and the determination of the transition from laminar to turbulent flow. Questions about the limits of laminar, desirable, time invariant flow patterns have been raised, but not answered, by the flow visualization studies completed.

---

* See REFERENCE section, Appendix D.

Concurrent with this effort, recently published work has [2] indicated that surface tension driven flow may have greater importance in float-zone crystal growth than previously realized. Remaining to be resolved in float-zone crystal growth are the proper identification of the relative importance of surface tension driven flow, forced convection flow, natural convective flow, and pure heat conduction in a useful growth process on Earth or in space.

A stepwise plan for future work to investigate crystal growth phenomena wherein low gravity conditions available in a space site may be used to advantage is presented. Most particularly, the plan calls for an investigation of the comparative merits of producing large crystals on Earth by the modified, off-set axis float-zone technique with the conventional colinear pulling technique which can produce very large crystals in space but not on Earth. This plan involves also research and development efforts of potential benefit to Earth-based crystal growing processes.

This study program has been sponsored by the George C. Marshall Space Flight Center, National Aeronautics and Space Administration, Huntsville, Alabama. Mr. M. Davidson is the COR director of the study. Dr. A.A. Fowle, Dr. J. S. Haggerty, Mr. R. R. Perron, Mr. P. F. Strong and Dr. J. L. Swanson of Arthur D. Little, Inc., are the investigators. Professor August F. Witt of M.I.T. and Mr. Niels Young have contributed as consultants.

TABLE OF CONTENTS

	Page Number
FOREWORD	iii
1.0 SUMMARY	1
1.1 PURPOSE AND SCOPE	1
1.2 RESULTS	2
1.2.1. Stability Experiments	2
1.2.2. Flow Visualization Experiments	2
1.2.3. Economics of Float-Zone Growth in Space	2
1.3 CONCLUSIONS AND RECOMMENDATIONS	3
1.3.1. Technological	3
1.3.2. Economic	4
1.3.3. Future Work	4
2.0 INTRODUCTION	6
3.0 TECHNICAL INVESTIGATION	8
3.1. STABILITY STUDIES	8
3.1.1. Introduction	8
3.1.2. Experimental Apparatus	9
3.1.3. Tests	10
3.1.4. Results	10
3.2. FLOW STUDIES	11
3.2.1. Introduction	11
3.2.2. Experimental Apparatus	11
3.2.3. Tests	13
3.2.4. Results	14
4.0 ECONOMIC IMPACT ANALYSIS	32
4.1. SCOPE	32
4.2. RESULTS	33
4.3. CONCLUSIONS	35

TABLE OF CONTENTS, (cont.)

	Page Number
5.0 FUTURE WORK	40
5.1. BACKGROUND	40
5.2. PROGRAM PLAN	41
5.2.1. Outline	41
5.2.2. Flow Visualization Studies	42
5.2.3. Surface Tension Driven Flow Study	42
5.2.4. Simulation of Zero-Gravity Crystal Growth Using a Small Scale Si Process	43
5.2.5. Other Zero-Gravity Experiments	43
APPENDIX A - PHOTOGRAPHIC TEST SYSTEM DESIGN	44
A.1. INTRODUCTION	44
A.2. OPTICAL DESIGN CONSIDERATIONS	44
A.3. PHOTOGRAPHIC APPARATUS	50
APPENDIX B - EFFECT OF GRAVITY AND LOCAL FLUID ACCELERATION ON THE ABILITY OF SMALL SPHERICAL PARTICLES TO GIVE AN ACCURATE TRACE OF THE LIQUID FLOW FIELD	54
B.1. GRAVITY EFFECT	54
B.2. ACCELERATION EFFECT	56
APPENDIX C - METHODS USED FOR ESTIMATING THE COST OF SI CRYSTAL PRODUCED ON EARTH AND IN SPACE	58
C.1. SCOPE	58
C.2. METHODS	58
C.3. BASIC CALCULATIONS	59
C.4. SUMMARY IMPACT ANALYSIS	63
APPENDIX D - REFERENCES	73

LIST OF FIGURES

Figure Number		Page Number
3.1	Stability Limits in Co-Rotation	18
3.2	Original Design of Experimental Equipment Planned for Flow Modeling Studies of Float-Zone Silicon	19
3.3	Experimental Equipment Modified to Bring Axis of Float-Zone Model Into the Vertical Plane	20
3.4	Close-up View of Plastic Rods Used to Contain Float-Zone Model	21
3.5	Comparison of Experimental Results and Theoretical Prediction of Co-rotation Stability Limit	22
3.6	Off-Axis Hollow Spindle Designed for Axial and Lateral Dark-field Visualization of Particle Pathlines in a Model Float-Zone	23
3.7	View of Final Design of Experimental Apparatus Showing Dark-field Flow Visualization Equipment Additions (One Camera of Stereoscopic Pair of Cameras Missing in this photograph)	24
3.8	Stroboscopic Tracking of Flow Visualization Particles in the Counter-Rotating Float-Zone Model	25
3.9	Stereoscopic Views of Particle Pathlines in the Float Zone Model When Counter-Rotating at ω = 0.5 Rev/Sec Using a Dilute Particle Solution	26
3.10	Stereopair Views of Particle Pathlines in the Float-Zone Model When Counter-Rotating at ω = 1.0 Rev/Sec Using a Dilute Particle Solution	26
3.11	Stereopair Views of Particle Pathlines in the Float-Zone Model when Counter-Rotating at ω = 1.25 Rev/Sec Using a Dilute Particle Solution	27
3.12	Stereopair Views of Particle Pathlines in the Float-Zone Model when Counter-Rotating at ω = 2.0 Rev/Sec Using a Dilute Particle Solution	27

Figure Number		Page Number
3.13	Stereopair Views of Particle Pathlines in the Float-Zone Model when Counter-Rotating at ω = 2.86 Rev/Sec Using a Dilute Particle Solution	28
3.14	Stereopair Views of Particle Pathlines in the Float-Zone Model when Counter-Rotating at ω = 5.0 Rev/Sec Using a Dilute Particle Solution	28
3.15	Stereopair Views of Particle Pathlines in the Float-Zone Model When Counter-Rotating at ω = 1.25 Rev/Sec Using a Concentrated Particle Solution	29
3.16	Stereopair Views of Particle Pathlines in the Float-Zone Model when Counter-Rotating at ω = 1.25 Rev/Sec Using a very Dilute Particle Solution	29
3.17	Approximate Pathline in Lower Rotating Water Cell	30
3.18	Estimated Velocity Distribution	31
4.1	Estimated Value of Single Crystal Silicon Substrate for Solar Cell or Single Rectifier	36
4.2	Estimated Value of a Single Crystal Silicon Substrate for MOS or IC	37
4.3	Estimated Value of Single Crystal Silicon Substrate for Bipolar IC	38
4.4	Maximum Potential Savings to Electronics Industry	39
A.1	Construction Showing the Refracted Rays of Light Within a Cylindrical Column of Water	52
A.2	System to Photograph a Particle in Dark Field Illumination	53
C.1	Estimated Yield of Sawing Process	70
C.2	Estimated Value of Earth Float-Zone Processed Wafers vs. Complexity of Final Application	71
C.3	Estimated Yield in Polished Wafer to Chip Process	72

LIST OF TABLES

Table Number		Page Number
C.1	Estimated Cost of Bare, Polished Si Wafer Produced on Earth	65
C.2	Estimated Cost of Bare, Polished Si Wafer Produced in Space	65
C.3	Estimated Cost of Finished Si Substrate for Solar Cell or Rectifier	66
C.4	Estimated Cost of Finished Si Substrate for MOS or IC	67
C.5	Estimated Cost of Finished Si Substrate for Bipolar IC	68
C.6	Estimated Economic Impact of Space-Based Production of Si Wafers by the Float-Zone Process	69

1.0 SUMMARY

1.1. PURPOSE AND SCOPE

The objective of this work was to evaluate and maximize the potential benefits of producing superior quality silicon crystals in a space environment by the float-zone process. A perceived benefit is the possibility of producing larger diameter crystals than can be achieved on Earth which may translate into less expensive crystal elements for final use. By incorporating relative rotation between the crystal and feed stock, forced convective currents may be induced in the melt which can result in a radial distribution of axial heat flux at the freezing interface which reduces grown-in stresses for crystals of the larger sizes that are possible to produce in a near-zero gravity environment. Also, the adverse effect of natural convection on the growth of crystals of uniform composition may be mitigated in the space environment. The scope of this program was, subdivided by task:

1) Examine the stability of silicon molten zones in configurations and under rotational conditions having promise for producing large, perfect crystals in a space environment using experiments based on scale modeling techniques.

2) Examine the circulation patterns within silicon molten zones in configurations and under roatational conditions selected to produce circulations most beneficial to the growth of large, near perfect crystals in the space environment using flow visualization methods applied to experiments based on scale modeling techniques.

3) On the basis of the results achieved above and from prior studies define the most promising configurations and process variables for the float-zone growth of a 6-inch or larger diameter silicon crystal. For this system, specify the expected velocity field within the molten zone and carry out a thermal analysis of the system to result in a definition of its temperature and heat flux distributions and heating requirements.

4) Recommend a research and development plan in a continuing program leading to a space experiment.

Although the original purpose of our investigation remained the same the scope was altered because of the influence of newly developed information resulting from our work. This new information forced the reconsideration of the technical foundations supporting the Work Statement of our contract. This new information also dictated that the most efficient allocation of contract funds would eliminate Task 3 and apply them to Task 4. Moreover, we decided that a more precise evaluation of the possible economic impact of space-manufactured single-crystal silicon by the float-zone process

was needed to provide a better foundation for our recommendations for further work. Accordingly, we made such a re-evaluation at no cost to the government.

1.2. RESULTS

1.2.1. Stability Experiments

The asymmetric stability limit for co-rotational float-zone crystal growth that was developed in our previous contract, and reported in the Interim Report [1] was experimentally verified in the present contract. Experimental data was taken from a float-zone scale model consisting of distilled water held by surface tension forces between the opposing flat surfaces of two rotating, precision plastic rods. The apparatus that held the rods was designed and constructed for accurate rod alignment while providing precision, adjustable speed regulation and a minimum of shaft vibration.

1.2.2. Flow Visualization Experiments

Further developments in the experimental technique and apparatus, established initially for the rotational stability measurements, resulted in informative flow visualization studies. Included in the major experimental developments were: 1) fabrication of a dark-field illuminator, 2) construction of a stereoscopic camera system, 3) creation of an electronic flash unit which established the directional or sense characteristics of tracer particle velocity, and 4) acquisition and use of wetting, non-agglomerating, polystyrene flow tracing particles.

Visual and photographic observations using this apparatus have confirmed that unique, time-invariant streamlines exist within the top and bottom cells of a counter-rotating float-zone model. The model once again consisted of distilled water suspended between equal-diameter, equal-counter-rotating rods with a common axis. Many of the streamlines could be described as a continuous helix-within-a-helix, with the number of helix spirals dependent on the rod rotation rate and initial particle position. Other streamlines appeared to orbit the mid-region of the counter-rotating cells. In addition, a unique, flat plane-of-symmetry separated the mirror image streamlines in the oppositely rotating cells. At higher rotation rates, several well-defined surface swirls were seen precessing about the circumference of the float-zone model, centered on the plane of flow symmetry. Very high rotation rates -- indicative of possible turbulent flow -- produced flow tracer motion too fast to be followed by eye or recorded on photographic film.

1.2.3. Economics of Float-Zone Growth in Space

An updated economic analysis of float-zone growth in single-crystal silicon in space has yielded several important results. These results apply to cases where the production of single crystal silicon in space is to be used by the electronics industry on Earth and therefore must compete economically with single crystal production on Earth by whatever method.

They do not reflect on the possible benefits of processing single crystal Si in space as a research endeavour, nor on the possible benefits of producing crystals in space for use in space. For instance, in the latter catagory, it may be beneficial to space process Si into solar cells for use in the photovoltaic version of SPS. These possibilities have not been examined, being outside the scope of our work. Moreover, no special value has been placed on Si crystals of superior quality nor on the possibility of reduced energy payback by utilization of the Sun as a source.

With these qualifications, we find that using near-term ($1000/kg) and long-term ($100/kg) transportation costs, clear economic justification was not shown for growing single-crystal silicon in space, when compared to Earth grown materials of comparable quality. A tenuous economic advantage of space-grown silicon can exist under assumed conditions that favor the space process: most importantly, low space transportation costs, equal capitalization, energy and labor costs, and the impossibility of producing vary large diameter single-crystal silicon wafers of equivalent quality on Earth in the next 20 years or so. We conclude that some new technology affecting the market must develop in order to realize a clear economic advantage resulting from the production of crystal Si in space by the float-zone process.

1.3· CONCLUSIONS AND RECOMMENDATIONS

1.3.1. Technological

From this past year's work we have reached several major conclusions:

- The stability limits imposed on the maximum size of grown crystals bound other more restrictive criteria governing optimal crystal growth operating conditions.

- The steady, well ordered circulation patterns of the type predicted as useful to stress-free, silicon crystal growth apparently persist only for Reynolds number (N_{Re}) less than about 200. However, the flow visualization studies completed to date are not quantitatively precise and require further work. In this low range, heat transfer by conduction dominates any forced convective flows induced by rotation of the silicon crystal and feed stock. In the sought for, desirable operating condition, heat transfer by forced convection dominates that due to conduction.

- It appears that, at the low range of Reynolds' numbers associated with the desired, steady, well ordered circulation patterns induced by rotation, flows induced by differences in surface tension forces (either due temperature or compositional changes within the melt) can become important.

- The appearance of surface flow swirls is an unresolved flow phenomenon which may influence the establishment of desirable float-zone crystal growth operating conditions.

These conclusions are based on the recent analytical work of Chang and Wilcox [2] and the experimental observations made under the present contract.

Our flow visualization studies have led to many of the useful results outlined above. The present limitation of the apparatus of most consequence is that present flow tracer reflectivity has not allowed photographic observations at high float-zone rotation rates (N_{Re}>200). The enhancement of the reflective properties of the particles by a suitable coating should allow observations of fluid behavior at these larger circulation rates. The experimental apparatus used to date has functioned well, has produced useful results, is available in a working condition with benefits from our experience relative to its operating characteristics. Its capabilities are far from exhausted.

1.3.2. Economic

From recent work we conclude that the economic benefits of space-processed, float zone single crystal silicon are tenuous. This recent assessment differs from that presented in October 1974 [1] and results from a quantitative consideration of the cost of space transportation, the time of possible introduction of space manufacture and the competition of other methods for crystal growth - which promise wafer sizes large enough to eliminate the hitherto perceived economic advantage of large size crystals made possible only in a space process.

Accordingly, we believe future work along the lines we have pursued has most potential benefit in the development of a better understanding of the physical processes at work in producing crystals from a melt by the most appropriate Earth-based or space-based process. This understanding can lead to the production of superior quality crystals on Earth and can provide a guide to producing crystals in space of a quality unobtainable on Earth because the detrimental effects of gravity induced natural convections in the melt can be avoided. This assessment takes no account of the value of superior quality crystals and/or the reduction of energy payback periods for crystal production using the Sun as an energy source. This deficiency should be remedied by further work.

1.3.3. Future Work

The objective of our recommended plan for future work is to develop the understanding and means to make better and more economical crystals grown from a melt in space or on Earth. It has elements of increasing complexity and cost to provide milestones for reconsideration of future work. These elements are:

- Conduct more experiments using improved versions of the flow visualization apparatus now useful in order to:

  1) Extend its visual range to higher flow velocities (perhaps in the turbulent regime) and thereby make reasonable judgments as to the practical use of these flows,

2) Make adjustments in the geometry of the apparatus to represent conditions of the newer, parallel, off-axis technique for growing large diameter, single-crystal silicon.

3) Compare results of tests representative of the conventional, colinear float-zone geometry (which can be utilized in space to produce large and, perhaps, a better quality product) and those representative of the newer off-axis growth method capable of growing large, single crystals on Earth.

- Conduct experiments for the purpose of assessing the importance of surface tension gradient driven flows in Earth and space-based crystal growth processes.

- Conduct silicon crystal growth experiments in our laboratories using the conventional colinear geometry on a model scale that makes gravity effects negligible. Compare the resulting crystal quality with that obtainable in the largest single crystal elements commercially available.

- On the basis of the above, design useful space experiments. This latter recommended work element would consider the possibilities of opportunities presented by zero-gravity airplane or rocket orbits or future shuttle flights whenever they occur in consonance with the progress of the work outlined above.

2.0 INTRODUCTION

There are several potential advantages of float-zone crystal growth: 1) whether gravity forces are present or not, higher purities are possible with containerless crystal growth processes from high temperature melts, 2) inherently uniform axial dopant levels result from a zone-leveling mode of growth, 3) as a consequence of the near weightless environment of a space laboratory, buoyancy-induced convection is effectively eliminated from the melt (lack of control over this transport mechanism is responsible for many common crystallographic defects), and 4) larger size crystals may be produced in space than on earth because of the absence of the destabilizing effects of gravity forces. Furthermore, larger crystals have the potential economic advantage of allowing the fabrication of large crystal elements and higher yields of acceptable crystal chips.

Our work for the period March 1974 to October 1974 led to an understanding of possible benefits from the production of single-crystal silicon in space, and these benefits were expressed in our Interim Report. The following is an outline of those perceived benefits.

In order to meet the goal of producing large crystals, it is necessary to overcome the deleterious effects of thermally-induced, residual stresses in the crystal that become emphasized with scale. An ideal solution to this problem is achieved if the conditions of the process are arranged to produce a freezing interface that is a plane perpendicular to the axis of growth.

In a first generation space laboratory for processing large Si crystals, the use of an incandescent heat source is envisioned. This source will heat the melt via radiation and, as the silicon melt is opaque to the emitted radiation, the heating will take place at the surface. In the absence of rotation, heat transport by solid conduction will convey heat to interior regions of the melt but this mechanism is inadequate for large diameter crystals.

Rotation of the crystal and feed stock provides a means for effecting "in-depth" heating of the melt zone via forced convection. Rotation also reduces the azimuthal temperature gradients that would exist in the absence of rotation. Relative angular rotational rates between the feed and crystal and/or different crystal and feed stock diameters result in circulating currents within the melt zone and attendant forced convective heat transport. The technological task that presents itself is to define the rotational rates and geometric characteristics of the crystal and feed stock that will result in the circulation currents that are most favorable for producing a stress-free crystal that is also free of crystallographic defects. Although rotation may be used to advantage to induce convective heat transport to the inner regions of the melt, it also results in destabilizing centrifugal forces and can produce periodic variations in the flow field within the melt zone. The type and degree of

rotation must, therefore, be established so that the stability limits of the melt are not exceeded and the spatial and temporal variations of velocity associated with the forced circulation currents within the melt are attenuated to the degree necessary to prevent variations in the solute concentration within the growing crystal.

From the past year's work, reported here, our ideas relating to the technology and economics of the processing of single-crystal silicon in space by the float-zone method have been altered in some major respects to be discussed. Consideration of these changes have led us to the conclusion that our present, and any future related work, has most potential benefit in the development of a better understanding of the physical processes at work in producing crystals from any growth process involving circulation.

3.0 TECHNICAL INVESTIGATION

3.1. STABILITY STUDIES

3.1.1. Introduction

Industrial float-zone crystal growth commonly employs a counter-rotational scheme. The advantages of this rotational mode include superior convective heat transport to and from the melting and solidification interfaces and the inherently stable nature of counter-rotation compared to co-rotation. If co-rotation at equal rotation rates are employed in float-zone crystal growth, the molten material would rotate as a solid body and could thus be subjected to the lowest order rotational failure mode. That is, because of everpresent crystal and feedstock axis assignments, a rotating liquid column would enter into an asymmetric shape similar to that of a sagging beam with hinged ends and ultimately would fly apart. For counter-rotation at equal rotation rates, there is a stationary, no-slip mid-plane of symmetry above and below which exist viscous shear planes which extend to the crystal and feedstock no-slip interfaces. Thus, for counter-rotation, the destabilizing inertial forces at the float-zone mid-plane are zero, contrasted with the co-rotational case where these forces reach the maximum value. Because of this fact, it is apparent that, for the same rotation rates, counter-rotation is the more stable operational mode.

At the present time there is no known theory of counter-rotational stability, while theories describing several modes of co-rotational stability do exist. [1] [3] Since the latter case of instability provides a conservative estimate of allowable crystal and feedstock rotation rates, it was deemed important to experimentally verify the available co-rotational stability criteria. It was recognized, however, that rotation rate set by co-rotational stability criteria, which is far lower than a counter-rotational stability limit, may exceed that for the transition from laminar to turbulent flow.

Figure 3.1 - adapted from the Interim Report [1] - shows three conditions of co-rotational stability: 1) the classical Rayleigh static stability criterion:

$$h/a \leq 2\pi$$

where h is the float-zone solidification interface spacing and a is the molten cylinder radius; 2) an axisymmetric perturbation criterion

$$h/a \leq 2\pi \left(\frac{\rho a^3 \omega^2}{\sigma} + 1\right)^{-1/2},$$

where is the liquid surface tension, ρ the liquid density, and ω the zone angular rotation rate; and 3) an asymmetric perturbation criterion

$$h/a \leq \pi \left(\frac{\sigma}{\rho a^3 \omega^2}\right)^{1/2}$$

As can be seen from Figure 3.1, the latter asymmetric stability criterion represents the lowest mode of float-zone failure in the range of values for h/a of practical interest. It is interesting to note that this type of failure has been observed in Skylab experiments. [4]

3.1.2. Experimental Apparatus

The experimental apparatus designed and constructed for initial float-zone modeling studies is shown in Figure 3.2. As may be seen, the cylinder of water representing the floating zone had a horizontal axis and was contained between rods mounted on the drive shafts of two opposing motors. Each motor had continuous control from 5 through 3000 RPM in either direction. The motors were bolted to lead-screw slides which, in turn, were mounted with provisions for adjustments to a large precision base. Through this design, the motor axes were precisely aligned, while the effects of deliberate axis misalignment on the float-zone model behavior could be studied. This design also allowed studies of various degrees of co-rotation and counter-rotation, and the influence of different float-zone model length-to-diameter ratios. Automatic sensing equipment utilizing light beam choppers, light-emitting diodes, photodetectors and digital frequency/period metering visually displayed the rotation rates of the motor shafts.

As indicated in the Interim Report [1] terrestrial float-zone models must be quite small (nominally 2.7-mm radius when using water as the test liquid) to minimize the influence of gravity on the zone shape and fluid flow field. The analytical work within the Interim Report could not, however, provide empirical design criteria to guide in the specification of motor shaft speed control requirements, fluid zone vibration tolerance, and acceptable axis misalignments. Because of the potential importance of each of these influences, the initial float-zone modeling apparatus was designed with as much precision as was practical. The motors were thus selected to provide better than 1% regulation in RPM, while numerous base adjustments were provided to allow fine positioning of shaft parallelism and colinearity, and for slide perpendicularity adjustments. In this way, the opposing shaft centerlines were ultimately adjusted to within about 0.001-inch. Finally, the use of the massive slides and a heavy mounting base provided a high degree of vibration attenuation. Initial experiments were expected to indicate whether greater vibration control was required.

Not shown in Figure 3.2 are the rods that adapted to the motor shafts and which approximated the solid interfaces bounding the water float-zone model. Following several preliminary tests with various kinds of wood, metal, and plastic, Lucite was selected as a suitable material.

Preliminary float-zone modeling tests were conducted using the apparatus illustrated in Figure 3.2. These tests clearly demonstrated a very noticeable asymmetric sagging of the water cylinder, even with 5-mm diameter holding rods and a rod spacing-to-diameter ratio near unity. It was thus decided to reorient the rotational axis into the vertical plane, as shown in Figure 3.3. Gravitational effects were not eliminated in this change, but were at least made symmetric with respect to the column's axis.

Additional operating experience with the apparatus indicated that the factory-machined flat spots on the motor shafts significantly lowered the alignment surface area with the slip-on Lucite rods. This loss in surface area resulted in significant misalignments between the axis of the motor shaft and the slip-on rod, even though the outside diameter of the rod was machined concentric with the inside diameter of the hole bored for the motor shaft. The resulting wobble in the two rotating rods was serious enough to establish disruptive vibration patterns in a water column placed between the flat surfaces of the rods. Elimination of this wobble was subsequently accomplished by machining the outside diameter and flat surface of the rod while the rod was in place on the motor shaft. The motor drives were used to spin the rods, and a specially modified lathe compound slide (which held a cutting tool) was bolted to the precision base. Figure 3.4 shows a close-up view of the machined-in-place Lucite rods.

Also shown in Figures 3.3. and 3.4 is the camera used to take initial photographs of the water float-zone model during stability studies. The camera is a Polaroid MP3 with a Rodenstock-Eurygon, 35 mm f/4.0 lens.

3.1.3. Tests

With the above mentioned operational difficulties overcome, float-zone model stability experiments were made. The tests undertaken concerned co-rotational stability since failure in two modes of this nature was analytically predicted in previous contract work [1] and in the published literature [3] (but remained experimentally unverified) and represents a conservative, lower stability limit in float-zone crystal growth.

3.1.4. Results

Figure 3.5 shows the results of the co-rotational stability experiments for the lowest order of failure. The photographic insert shows the water column at the condition of imminent failure. Shortly after the photograph was taken a large particle of liquid was ejected from the column; however, part of the column survived.

As can be seen in Figure 3.5 the co-rotational stability data is in good agreement with theory. This data was obtained using distilled water suspended between equal diameter rods having colinear axes and the same angular velocity. The space between the rods was filled using a hypodermic syringe, followed by column height adjustments until a near straight-sided water cylinder was produced.

The circled data points denote the condition when the liquid cylinder became unstable and flew apart. Although there is some scatter in the data, no points fell below the critical limit predicted by theory.

The span of h/a in Figure 3.5 represents the operational range of the apparatus when the column radius equalled about 2.6 mm. h/a ratios smaller than about 0.6 required angular velocities greater than that possible with this system (3000 rpm), while h/a ratios larger than about 1.6 led to appreciable slumping of the water column. We believe that the data in Figure 3.5 provides sufficient corroboration of the co-rotational stability theory for practical application.

Several studies of counter-rotation instability indicated that, given the same geometries used in the co-rotational experiments, column stability was present almost up to the maximum speed of the motors (about 3000 rpm). Intense bearing noise and vibration was evident at these high rotation rates and thus may have presented an unnatural and non-reproducible influence on the stability of the column.

In summary, the most severe theoretically predicted limits for the stability of the molten zone of a float-zone Si crystal growing process in space has been verified. Moreover, these limits allow the growth of very large diameter crystals as predicted in the Interim Report [1]. Within these limits of size many more important considerations for more perfect crystal production must be addressed as discussed elsewhere.

3.2. FLOW STUDIES

3.2.1. Introduction

In order to visualize the flow fields in our model of a floating zone melt induced by various conditions of rotation of the crystal and feed stock (models) we introduced small tracer particles and photographed them using an optical system consisting of an intense source of light arranged to give dark field illumination and cameras capable of stereoscopic flash photography. We also made direct sightings by eye through a binocular microscope providing an enlarged view of the model molten zone.

3.2.2. Experimental Apparatus

The experimental apparatus shown in Figures 3.3 and 3.4 proved to be adequate for the rotational stability studies discussed in the last section, but required additional modifications for photographic mapping of flow streamlines. Initial attempts at this mapping using incandescent and stroboscopic light sources directed perpendicular to the water column's axis, while also viewing the motion of flow-tracking particles from a similar orientation, produced unsatisfactory results. The problem encountered was that insufficient light energy was introduced into the

water column so as to be able to resolve the small flow tracking particles, simultaneously avoiding light refraction and reflection into the camera lens. These problems were ultimately overcome through the additional apparatus modifications shown schematically in Figure 3.6.

As shown in Figures 3.6a and 3.6b, the top motor drive was altered to accommodate a new "side-arm" hollow spindle. This new mechanism provided operational flexibility unavailable with the earlier apparatus. Several of the important features included the new ability to provide dark field illumination of the flow tracking particles, inserted into the water column, and the ability to view the flow field along the column's center line. Through the latter method, refraction-induced distortions of true particle position were removed.

The side-arm spindle was designed to be a "strap-on" addition to the original apparatus so that flow visualization studies could proceed with the minimum of interruption. Of particular concern in the spindle design, as in the original apparatus design, was the minimization of vibrations transmitted to the rotating water column.

Figures 3.6a and 3.7 show the side-arm spindle set-up for axial illumination and lateral flow visualization. As seen, light enters the hollow spindle and impinges on an optical-grade Lucite window which also serves as the top supporting rod of the water float-zone model. Except for the flat rod surface, the exterior of the Plexiglas window was blackened to reduce extraneous light. The bottom rod was also blackened for similar reasons. Figure 3.8 is an example of a dark-field photograph resulting from operating in this arrangement.

In Figure 3.6b can be seen the equipment arrangement which allowed axial examination of the flow field in the water float-zone model. By adjusting the position co-axial microscope objective within the hollow spindle, and proper selection of the focal length of the lens, it was possible to track flow tracing particles in either the top of bottom zones of motion.

Figure 3.7 shows several other new major additions to the experimental float-zone modeling apparatus. One of two 35 mm single-lens reflex cameras can be seen which were mounted on a frame oriented with the cameras' optic axes at right angles to the axis of the water column. These cameras subtended a 30° angle and thus provided a stereoscopic view of the flow tracking particles so that particle positions and velocities (magnitude and direction) within the float-zone model could be determined. Details of the design analysis of the photographic test system are provided in Appendix A.

The second major piece of equipment added to the experimental apparatus was a high-intensity, stroboscopic xenon flash light source. Together with the stereopair cameras, this light source allowed the photographic determination of particle position and velocity. Particle direction is established by three light flashes with uneven time pauses between flashes. Figure 3.8 illustrates the results of using this system. (Note that the

light source in Figure 3.8 was directed down the axis of the water column, as shown in Figure 3.7a, to permit dark-field illumination.) In Figure 3.8, flow tracking particles can be seen in three successive positions as a result of an 80 ms second pause followed by a 40 ms pause between light flashes.

The third major addition to the experimental apparatus was a tungsten-halogen, incandescent (projector lamp) light source and an adjustable dc power supply for the lamp. This incandescent lamp was attached to a specially constructed, adjustable fixture, so that the lamp could be used to illuminate the water float-zone model for dark-field flow visualizations. Important features of this lamp include its infrared transparent reflector and its large output of visible light. In this way, significant advances were made possible in photographing small particles used in flow visualizations, without over-heating the rotating zone of water. Extra protection against heating the water column was obtained by placing a piece of heat reflecting glass between the projector lamp and the water zone. Figures 3.9 through 3.16 result from the use of the incandescent light source.

3.2.3. Tests

Several very important elements in the production of photographs such as Figures 3.8 to 3.16, which document flow streamlines and cells, was the identification and development of suitable light scattering particles, and the development of methods of particle insertion into the water column. The most successful particles used to date were 3 to 10 μm diameter, "Aminex" polystryene spheres. These particles had an anti-coagulant surface treatment which prevents particle agglomeration when dispersed in water. Earlier visualization attempts with diluted water-based poster paint and alumina particles were unsuccessful because the particles did not wet well, causing them to reside on the free surface of the rotating water column.

The Aminex spherical particles were placed into the water float-zone model in several ways. Each method had advantages for revealing different aspects of the flow. One simple, but difficult to control, technique was to inject various dilutions of the particles into the water column using a very fine hypodermic syringe. This injection was done with the column in rotation and at rest. Starting with the column at rest, the bottom rod was rapidly rotated to get the particles stirred up and into a region slightly above the bottom rod surface. (The model of the crystalline fed stock.) This high rotation rate was maintained only for several seconds so that the whole column would not be clouded with particles. When each

motor controller was next adjusted to the desired setting, one could clearly see the formation of flow streamlines and cells and a flat midplane of symmetry. Because of large velocity gradients and shear forces at this midplane, particles often carried over into the top zone to reveal flow cells in that region.

A second method of flow visualization was to introduce the tracer particles into a column of water already rotating. Transient streak lines were at first evident, followed by the clear evidence of flow cells and streamlines at steady state conditions.

The polystyrene spheres were primarily useful in mapping stream velocities corresponding to rotation rates below approximately two per second (for a water column having about a 5 mm diameter and a 3.5 mm height). Above this rotation rate, the particles moved too fast to be photographed. Since streamline mapping at higher rotational rates was desired, additional effort was expended to improve the reflectivity of the tracer particles. As mentioned in Appendix A, progress was made in selecting nickel-plated, hollow glass spheres so that their average density would allow the spheres to be nearly buoyant in water. These particles have not yet been screened for size, and have only been used in preliminary visual flow studies. They did appear significantly brighter than the polystyrene spheres and thus represent prime candidates for tracing streamlines in future studies.

3.2.4 Results

An important result of the present flow visualization studies was the experimental demonstration of the existence of time-invariant, axisymmetric streamlines, and the presence of a flat, horizontal plane of symmetry between the top and bottom zones of a vertical counter-rotating water column. The existence of the above flow phenomena had been predicted as beneficial to the production of single crystal material with a minimum of stress-related physical site defects. The Reynolds number range for this laminar, well ordered, Taylor-Proudman cellular structure could not be predicted with any precision.

Beyond the experimental establishment of time-invariant and spatially symmetric streamlines, preliminary visual measurements were made of the rotational rates under which the streamlines were distinctly visible. At higher rotational rates the flow became visibly confusing, which may be an indication of a transition of the flow into the turbulent flow regime, but we have no certain evidence of this. For equal diameter, counter-rotating coaxial rods having a diameter of about 5 mm and a gap of about 3 mm, distinct streamlines existed when the rotational rate was less than approximately 5 revolutions per second. The rotational rate of 5 rps corresponds to a Reynolds number, based on the peripheral speed of the model crystal and feed stock of 214. At this low rate, counter-rotational stability of the float-zone model was never in question. Thus, if the interpretation of these observations is correct, the transi-

tion from laminar to turbulent flow probably represents a significantly lower operating limit than stability for float-zone single-crystal growth.

Figure 3.8 is one photograph from a stereo-pair of photographs produced using the stroboscopic flash equipment and cameras briefly described above. The cameras' axes subtended a 30° angle, while the time pauses between the three successive light flashes was 80 ms and 40 ms, respectively. With stereopairs of photographs it is thus possible to determine both particle position and velocity. Quantitative streamline mapping is incomplete at this reporting time, due to needed improvements in the optics of the second camera, and improvements in particle reflectivity and size. These improvements could not be completed within the present work effort.

Beyond stroboscopic particle tracking considerable progress was made in photographing particle streaklines (which are, for steady flow, also streamlines and pathlines). Figure 3.9 through 3.14 represents the results of a test in which the only changing independent variables were the shaft rotation rate and the length of time the camera shutter remained open. Particle concentration was held constant. The objectives of these tests were: 1) to determine the character of the streamlines as a function of rotation rate, 2) to verify that a streamline was time invariant and reproduced itself for constant rotational rates, and 3) to establish quantitatively the transition range from laminar to turbulent flow.

Direct visual interpretation of the photographs in Figures 3.9 to 3.14 without additional data processing is extremely difficult. As discussed in Appendix A, light refraction at the front surface of the water column significantly distorts the true position of a particle residing in the rear half of the column. Furthermore, because of this distortion there are rear regions where particles can reside totally hidden from an external observer. To complicate the situation further, light refraction at the front surface creates a brighter image from a particle residing in the rear region than one in the front region. Particle position in the front region is accurately portrayed in the photographs due to small refraction effects at the water interface.

It is clear from viewing Figures 3.9 through 3.14 that the experimental objectives of the flow visualization studies were not totally satisfied. Low reflectivity of the polystyrene tracer particles limited the ability to track particles at high shaft rotation rates. Further experimentation will be required to photographically document pathline and streamline reproducibility particularly at higher rotational rates. In spite of the lack of photographic evidence, however, numerous visual observations have confirmed that time after time the tracer particles traverse identical streamlines, at least for the Reynolds' range less than about 200.

One of the more interesting results from the experiment underlying Figures 3.9 through 3.14 was the observation of surface swirling phenomena. Figures 3.13 and 3.14 place in evidence examples of the observed behavior. Two, and sometimes, three, swirls have been seen which precessed slowly about the column's circumference, centered at the plane of flow symmetry. (The flow plane of symmetry was higher in elevation than the geometric plane of symmetry due to the noticeable slump in the water column.) This surface swirling was noted earlier, but was then attributed to non-wetting, agglomeration particles driving the flow from the free surface of the water column. Since the polystyrene particles used in the current experiments had an anti-coagulant treatment and wetted well, it thus appears that surfaces whirling is a natural effect produced in counter-rotating columns of liquid, and may persist throughout the laminar flow regime. The precessional rate of the swirls depended on the mismatch in top and bottom rotation rates and could be altered by the experimenter. The surface swirling phenomena was unexpected. Nothing hinting at such behavior has been suggested in the literature of crystal growth fluid dynamics. The closest known analog in nature seems to occur in the field of astronomy and astrophysics: the great red spot of Jupiter.

Since the observed surface swirls were time invariant, they occurred, by definition, in the laminar flow regime. Physics dictates that if the surface flow is laminar, the core flow must be laminar. Thus, from this sequence of photographs, laminar flow exists at least up to 5 rev/sec (corresponding to the Reynolds number of 214). The surface swirling represents a flow phenomenon not originally considered in the concept of the present work effort, and its quantitative impact on the overall transport of heat and the resulting float-zone crystal growth behavior has not yet been assessed.

Figures 3.15 and 3.16 demonstrate clearly the influence of tracer particle concentrations on observation of the spinning water column. (Also note that the rotational rate is the same as in Figure 3.11). As may be seen in Figure 3.15, two types of streamlines seem to exist simultaneously. One type of streamline is a coil within a coil, and extends from the flow midplane of symmetry to the rotating rod surface. The second kind of streamline appears to represent a circumferential orbiting motion with little axial or radial displacement in between the coils, thus signalling a relatively stagnant flow region in respect to radial and axial flow velocities.

From direct observations of flow tracking particles and the examination of numerous photographs similar to Figures 3.15 through 3.16, it has been possible to qualitatively map the flow field in an equal diameter, counter-rotating float-zone model at Reynolds' numbers less than 100. Figures 3.17 and 3.18 represent preliminary efforts.

The pathline shown in Figure 3.17 follows from direct visual tracking of one isolated particle at a very low shaft rotation rate. Particles' paths in a different streamline will, in general, appear different, and streamlines at higher rotation rates will also be quantitatively different. Nonetheless, Figure 3.17 is respresentative of the generally complex flow pattern within the float-zone model operating at low Reynolds numbers.

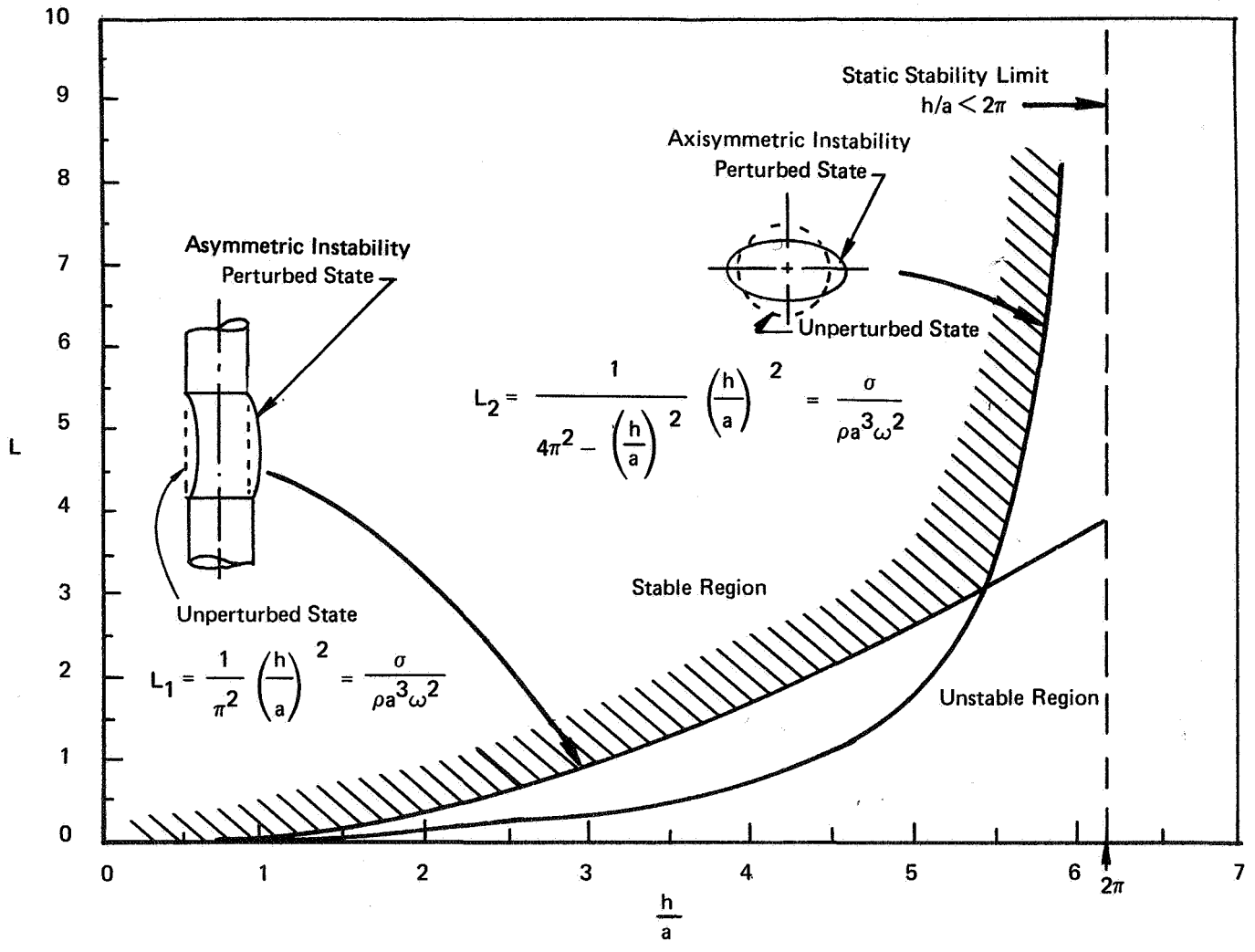

FIGURE 3.1 STABILITY LIMITS IN CO-ROTATION

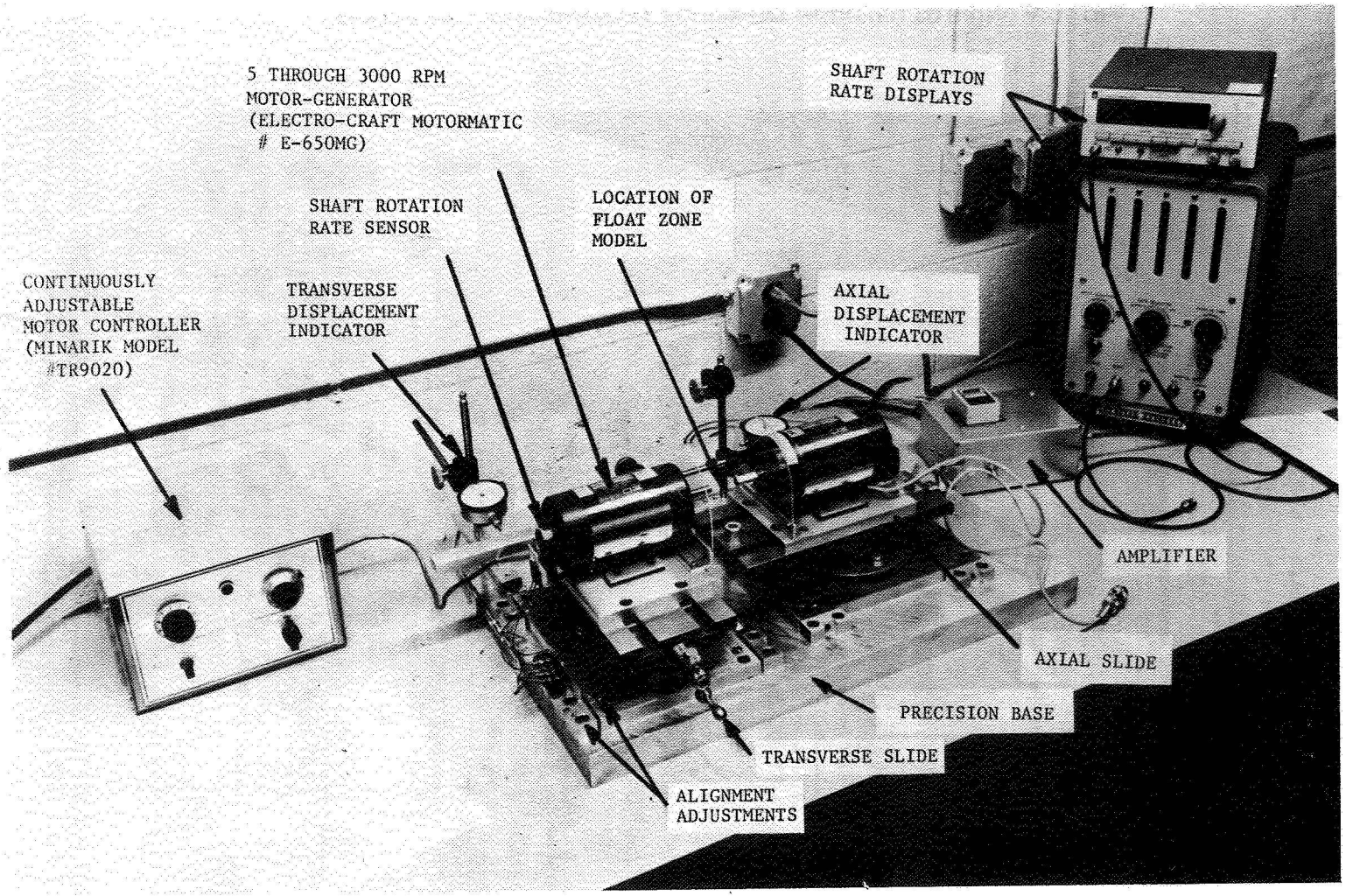

FIGURE 3.2 ORIGINAL DESIGN OF EXPERIMENTAL EQUIPMENT PLANNED FOR FLOW MODELING STUDIES OF FLOAT ZONE SILICON

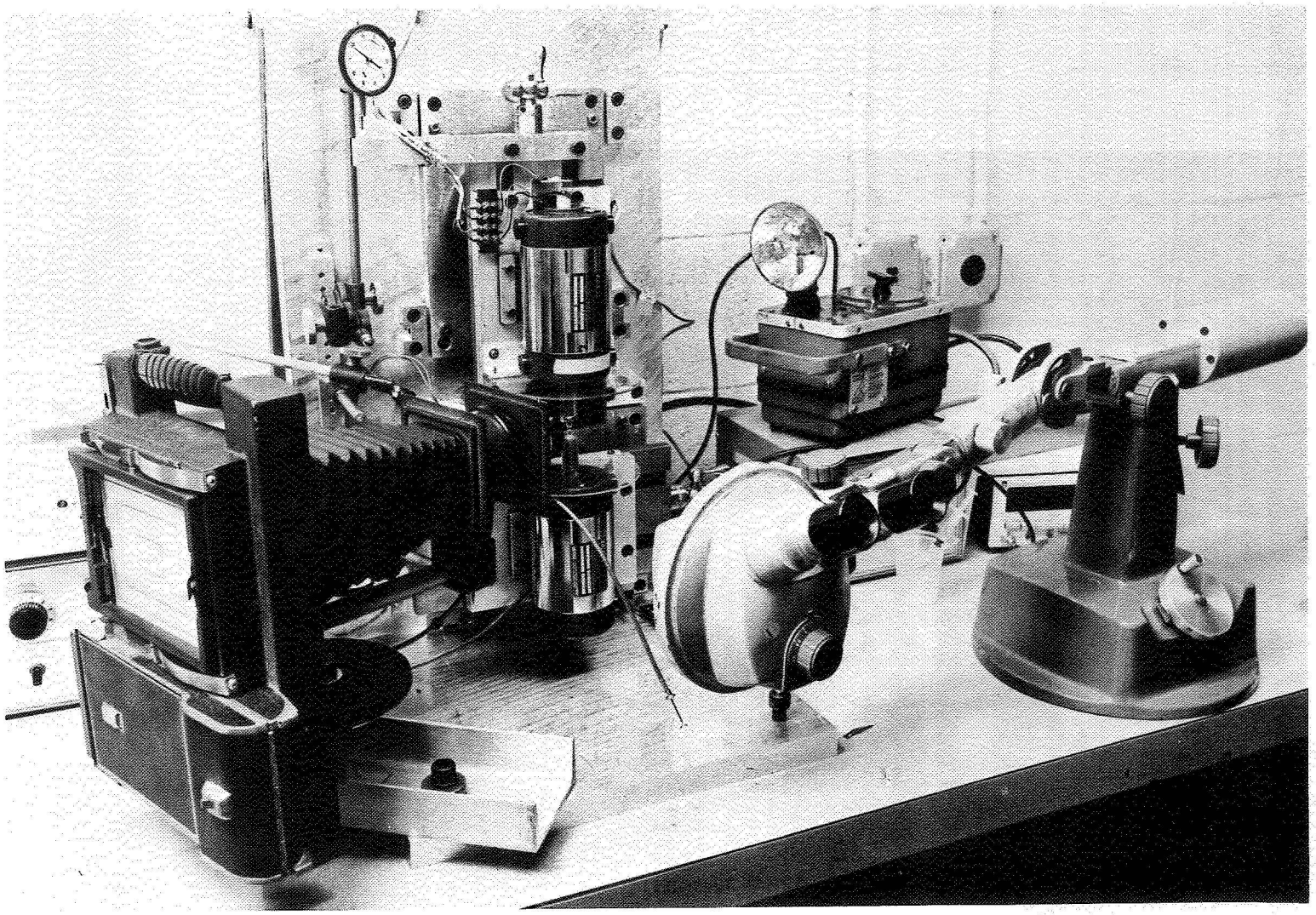

FIGURE 3.3 EXPERIMENTAL EQUIPMENT MODIFIED TO BRING AXIS OF FLOAT ZONE MODEL INTO THE VERTICAL PLANE

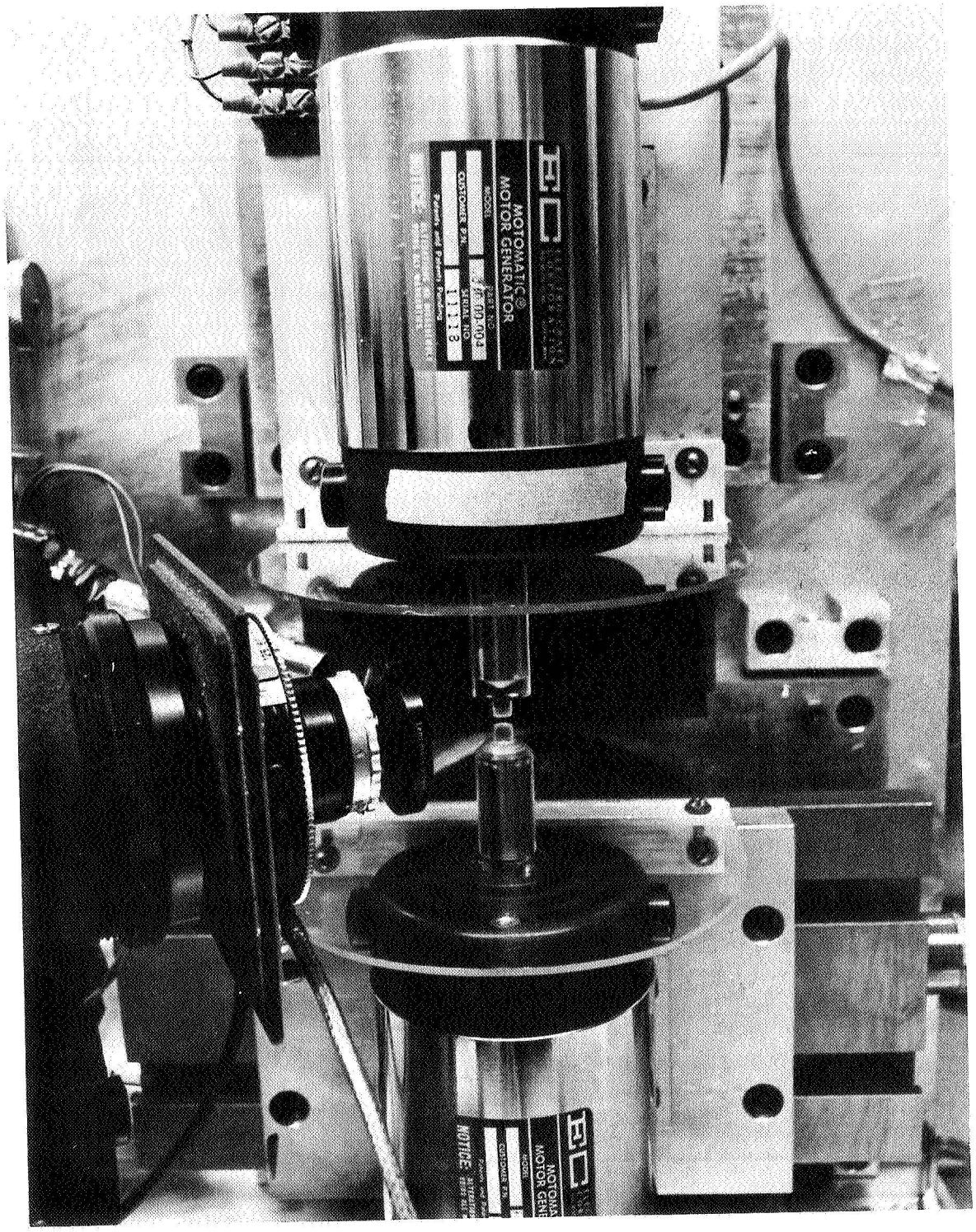

FIGURE 3.4 CLOSE-UP VIEW OF PLASTIC RODS USED TO CONTAIN FLOAT ZONE MODEL

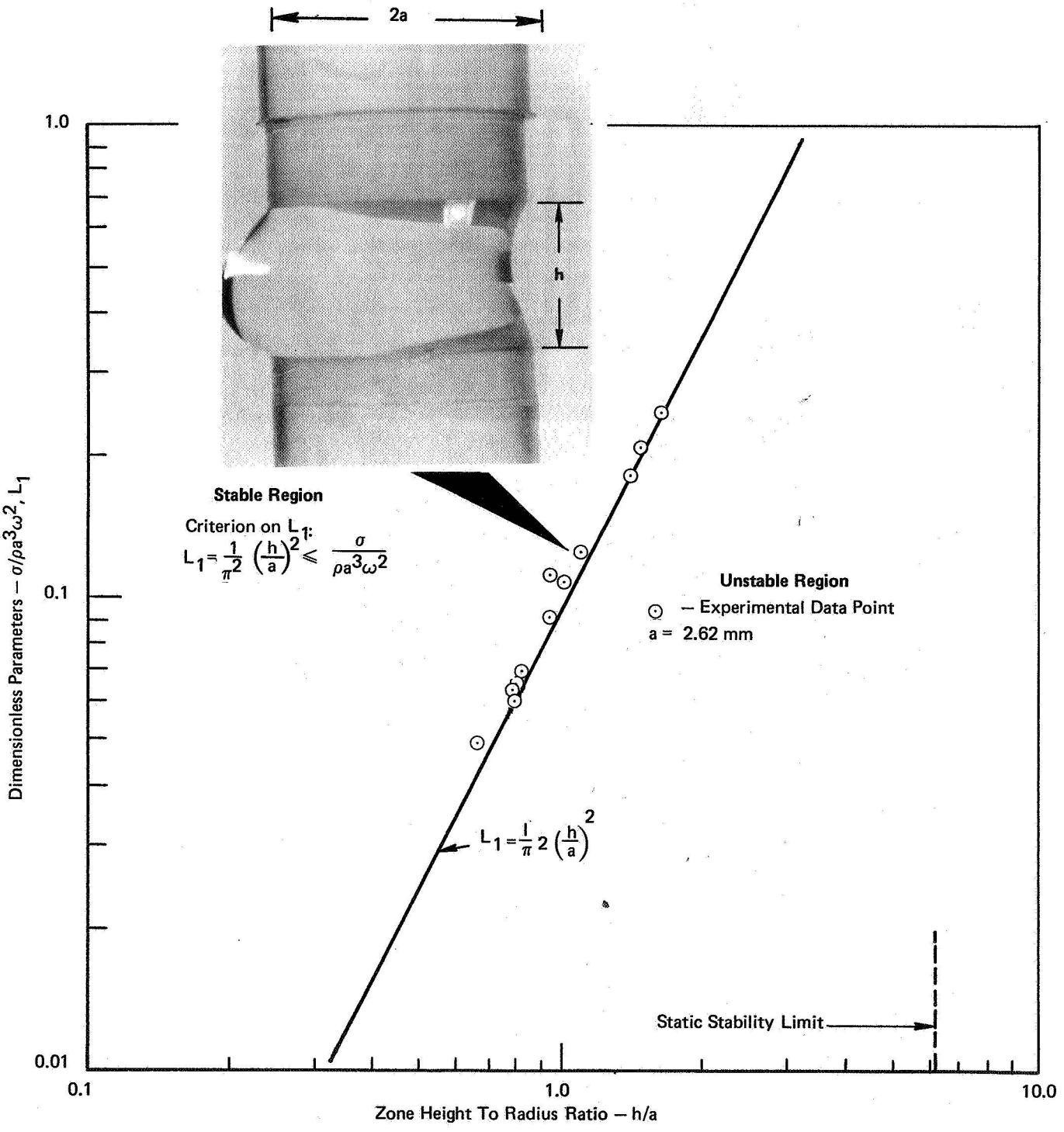

FIGURE 3.5 COMPARISON OF EXPERIMENTAL RESULTS AND THEORETICAL PREDICTION OF EQUAL DIAMETER, CO-ROTATION STABILITY LIMIT

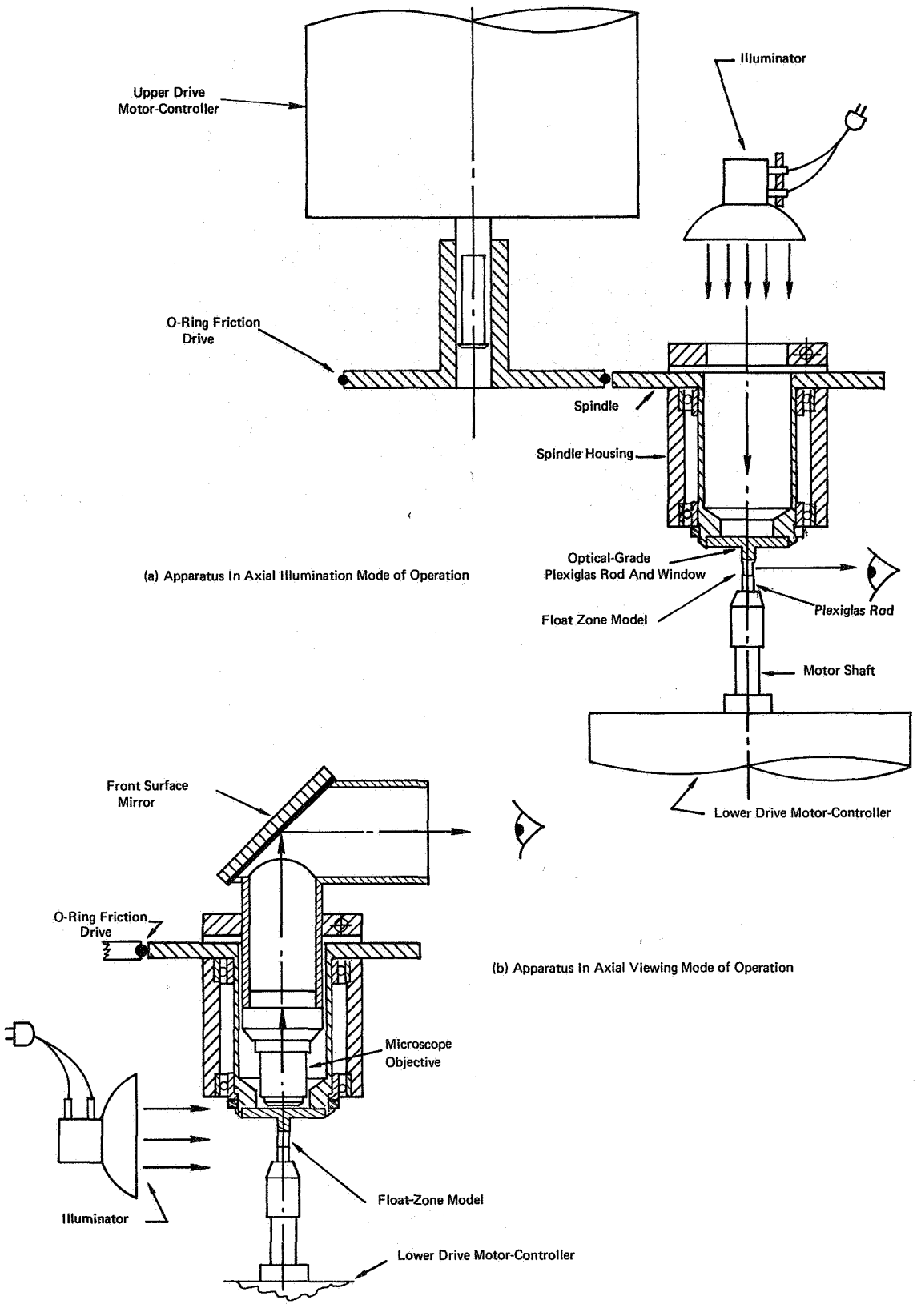

FIGURE 3.6 OFF-AXIS HOLLOW SPINDLE DESIGNED FOR AXIAL AND LATERAL DARK-FIELD VISUALIZATION OF PARTICLE PATHLINES IN A MODEL FLOAT-ZONE

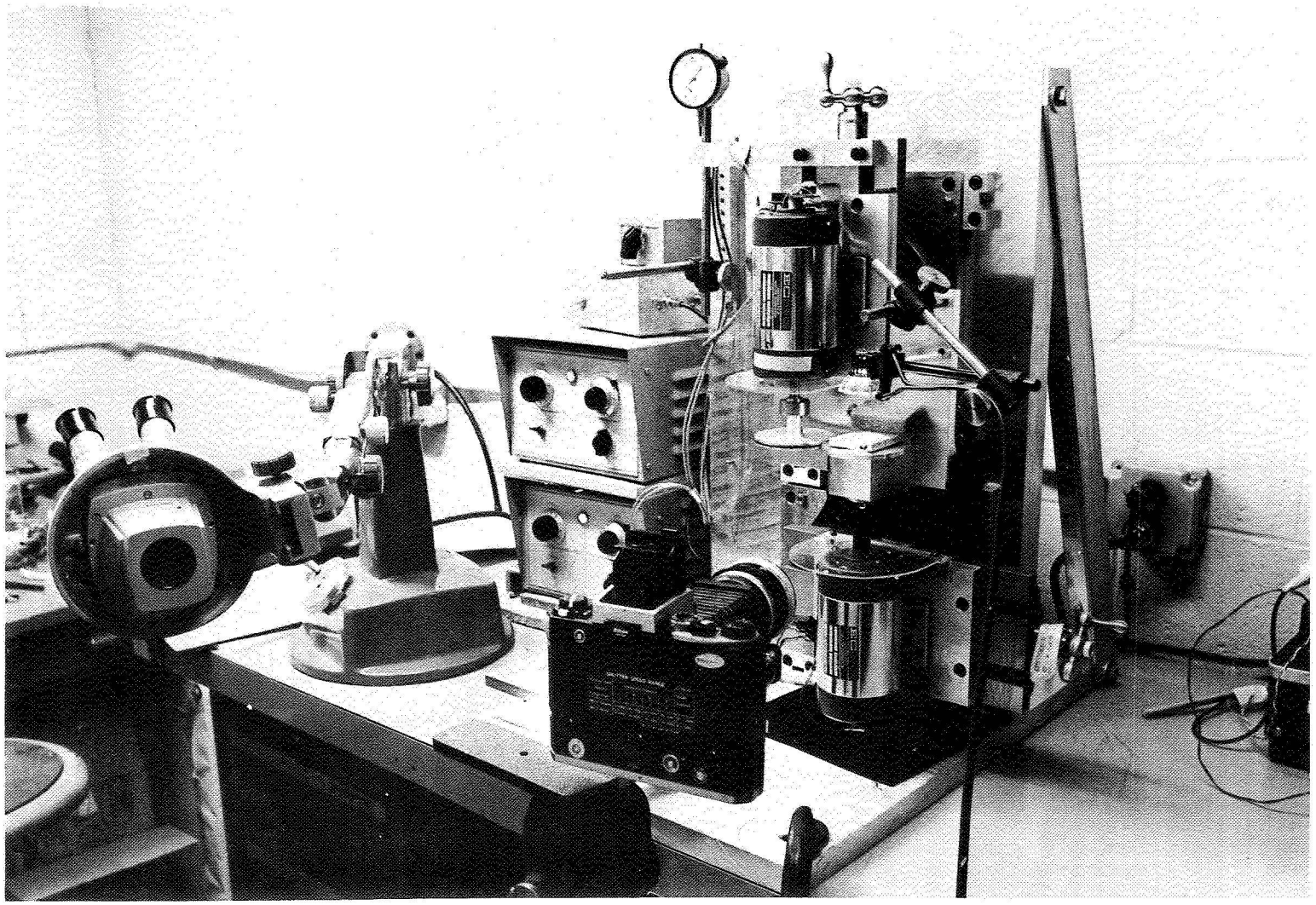

FIGURE 3.7 VIEW OF FINAL DESIGN OF EXPERIMENTAL APPARATUS SHOWING DARK-FIELD FLOW VISUALIZATION EQUIPMENT ADDITIONS (ONE CAMERA OF STEREOSCOPIC PAIR OF CAMERAS MISSING IN THIS PHOTOGRAPH)

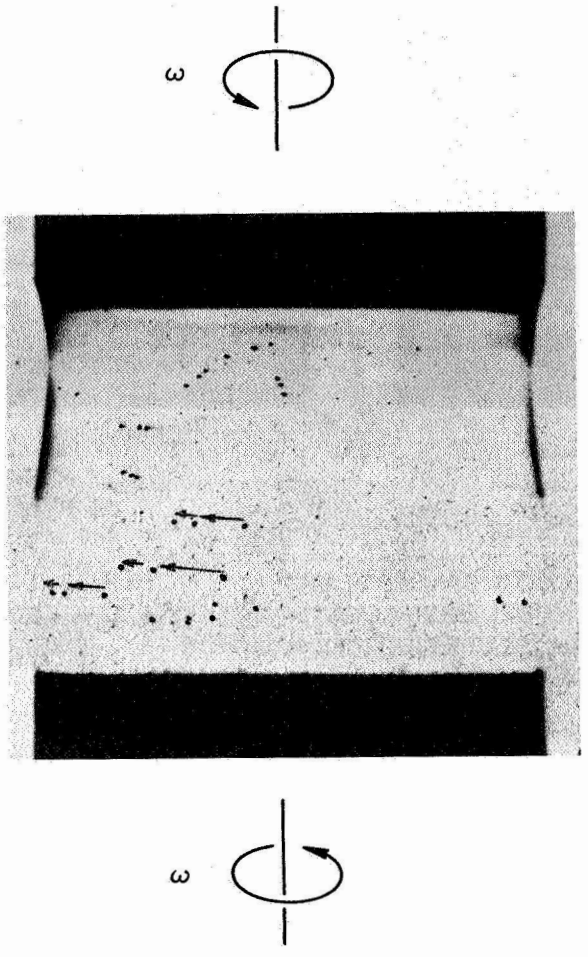

FIGURE 3.8 STROBOSCOPIC TRACKING OF FLOW VISUALIZATION PARTICLES IN THE COUNTER-ROTATING FLOAT ZONE MODEL

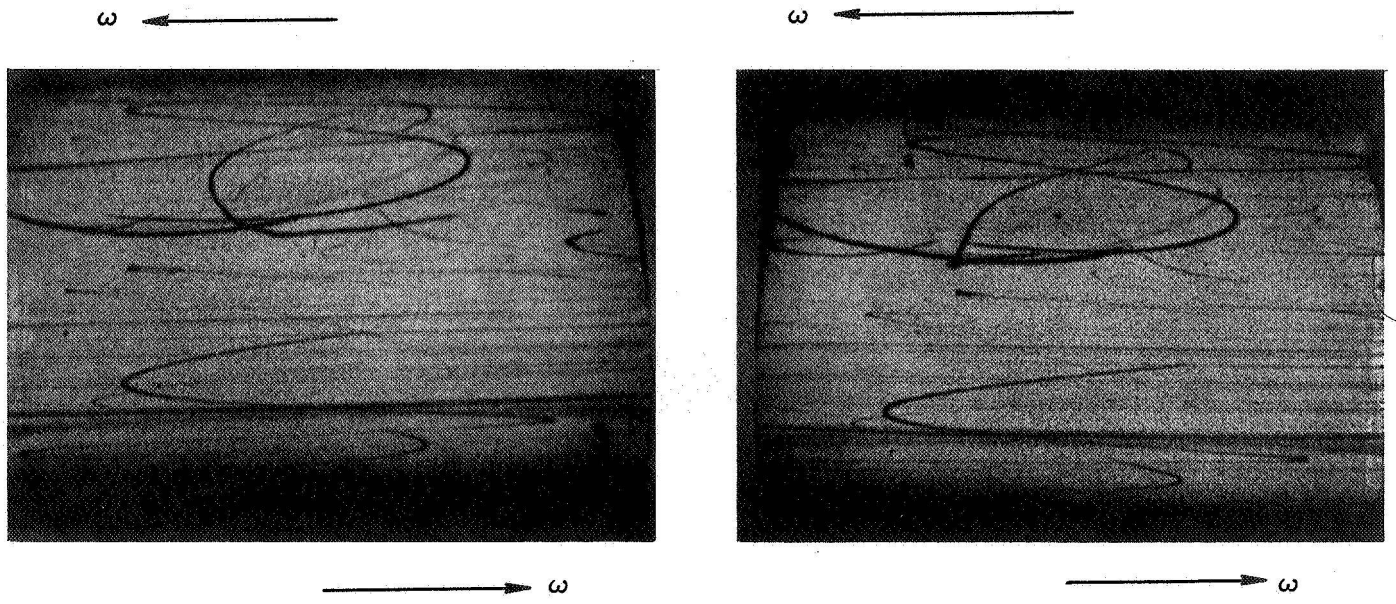

(a) Left Camera View

(b) Right Camera View

FIGURE 3.9 STEREOSCOPIC VIEWS OF PARTICLE PATHLINES IN THE FLOAT ZONE MODEL WHEN COUNTER-ROTATING AT ω = 0.5 REV/SEC USING A DILUTE PARTICLE SOLUTION

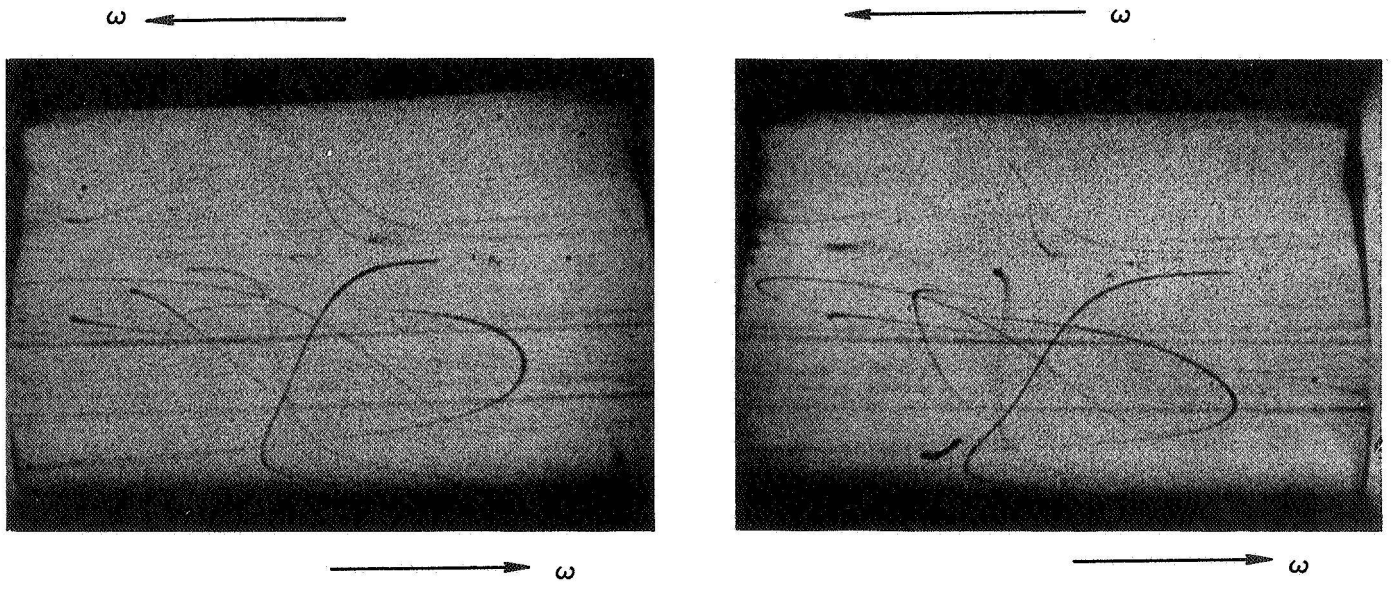

(a) Left Camera View

(b) Right Camera View

FIGURE 3.10 STEREOSCOPIC VIEWS OF PARTICLE PATHLINES IN THE FLOAT ZONE MODEL WHEN COUNTER-ROTATING AT ω = 1.0 REV/SEC USING A DILUTE PARTICLE SOLUTION

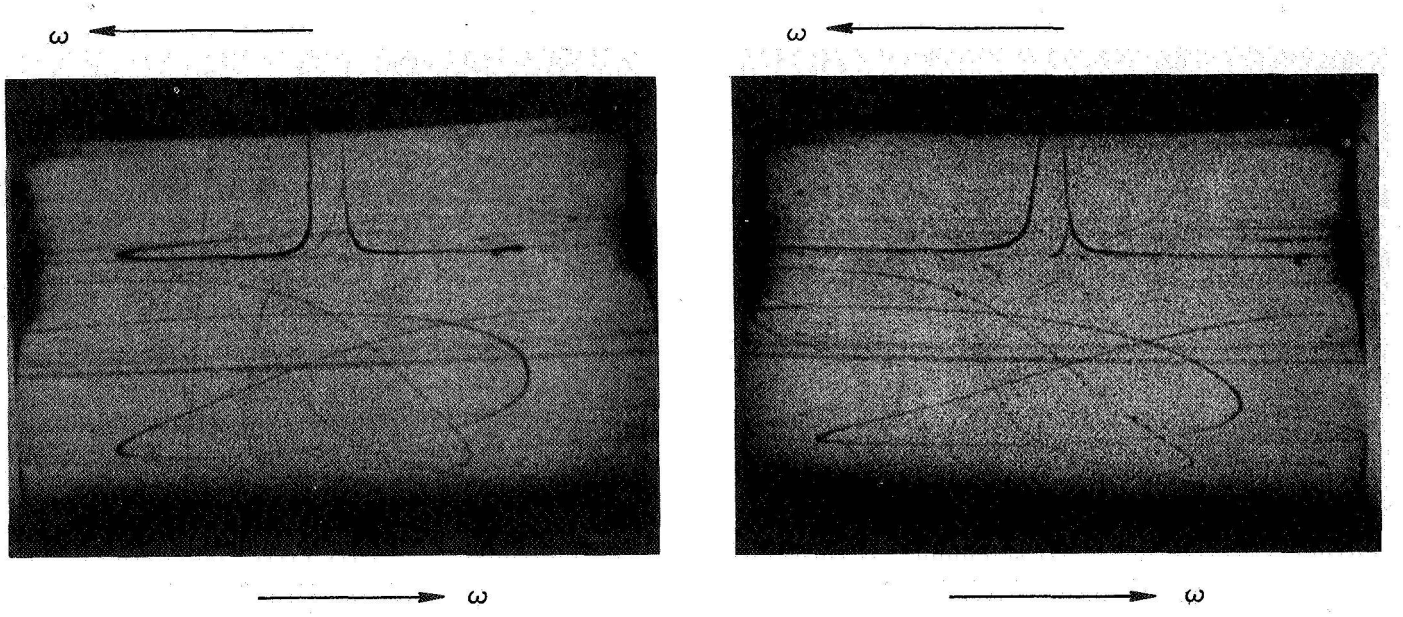

(a) Left Camera View (b) Right Camera View

FIGURE 3.11 STEREOPAIR VIEWS OF PARTICLE PATHLINES IN THE FLOAT ZONE MODEL WHEN COUNTER-ROTATING AT ω = 1.25 REV/SEC USING A DILUTE PARTICLE SOLUTION

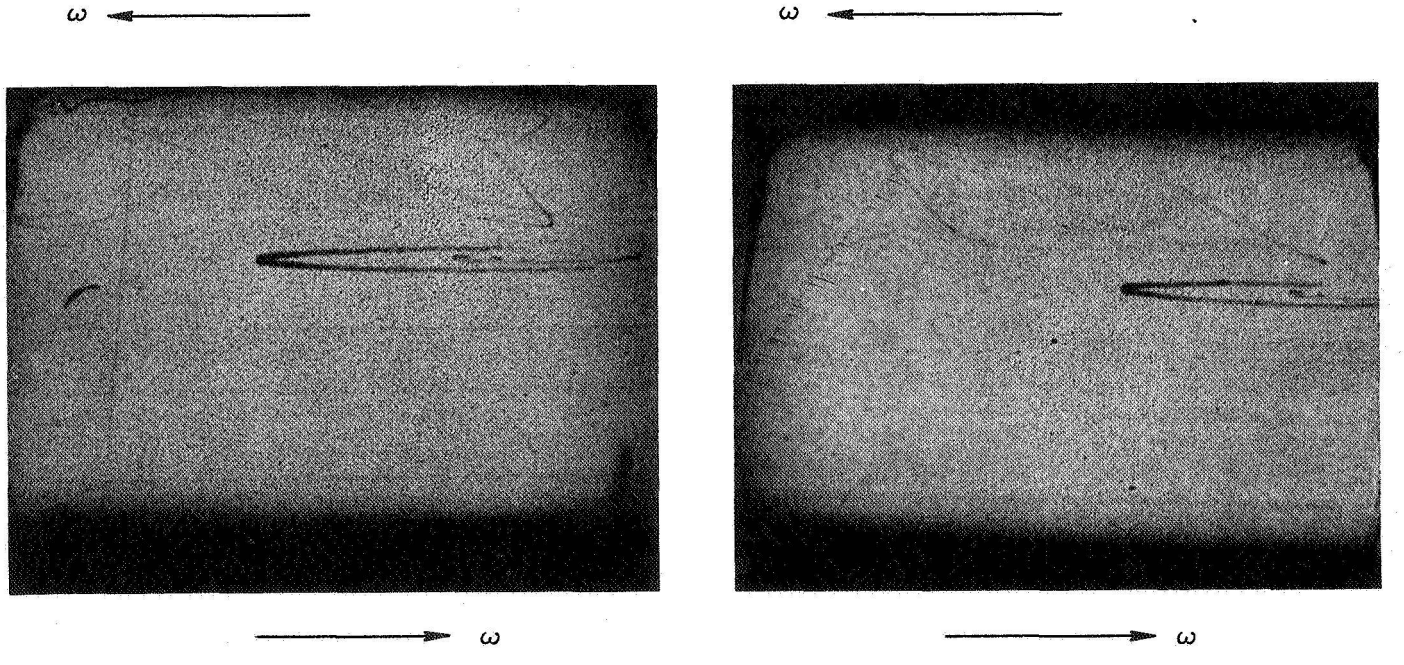

(a) Left Camera View (b) Right Camera View

FIGURE 3.12 STEREOPAIR VIEWS OF PARTICLE PATHLINES IN THE FLOAT ZONE MODEL WHEN COUNTER-ROTATING AT ω = 2.0 REV/SEC USING A DILUTE PARTICLE SOLUTION

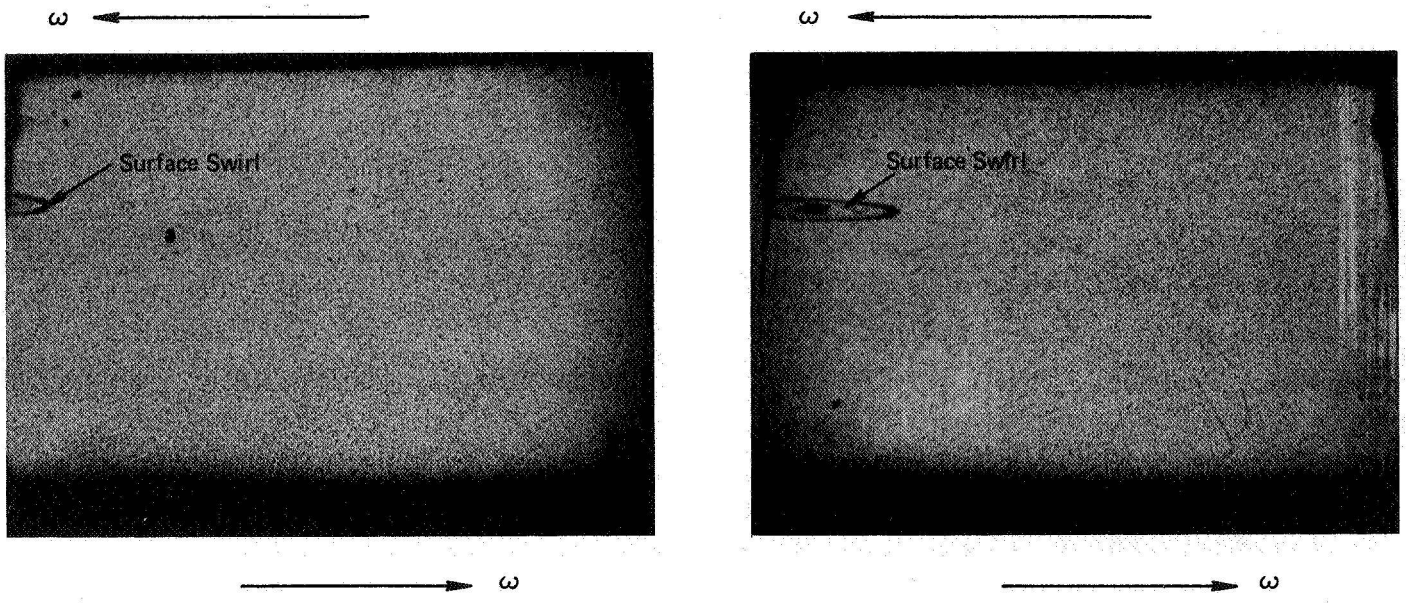

(a) Left Camera View

(b) Right Camera View

FIGURE 3.13 STEREOPAIR VIEWS OF PARTICLE PATHLINES IN THE FLOAT ZONE MODEL WHEN COUNTER-ROTATING AT ω = 2.86 REV/SEC USING A DILUTE PARTICLE SOLUTION

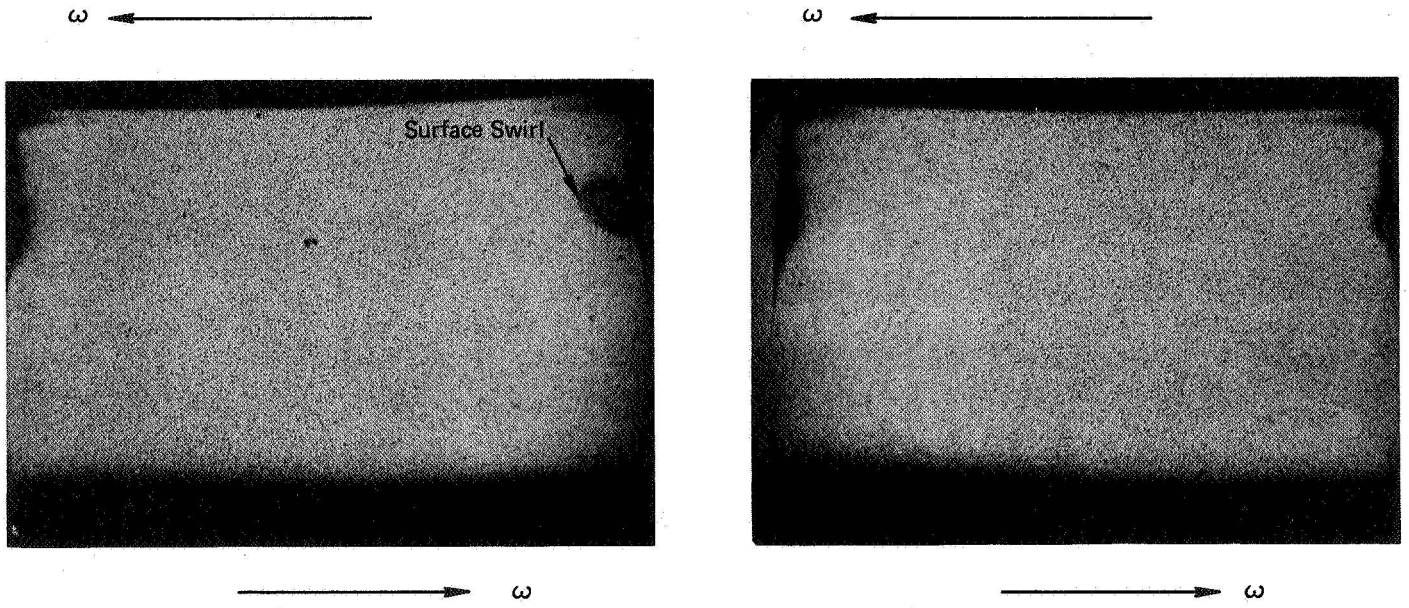

(a) Left Camera View

(b) Right Camera View

FIGURE 3.14 STEREOPAIR VIEWS OF PARTICLE PATHLINES IN THE FLOAT ZONE MODEL WHEN COUNTER-ROTATING AT ω = 5.0 REV/SEC USING A DILUTE PARTICLE SOLUTION

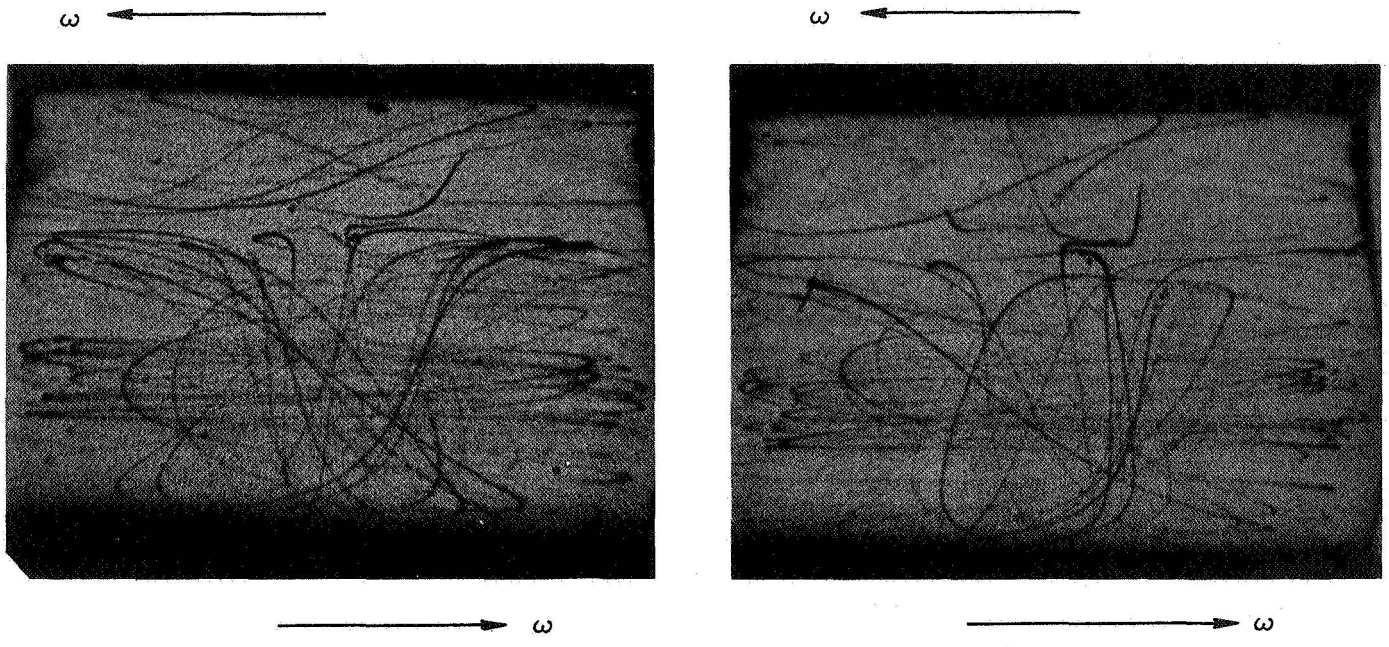

(a) Left Camera View

(b) Right Camera View

FIGURE 3.15 STEREOPAIR VIEWS OF PARTICLE PATHLINES IN THE FLOAT ZONE MODEL WHEN COUNTER-ROTATING AT ω = 1.25 REV/SEC USING A CONCENTRATED PARTICLE SOLUTION

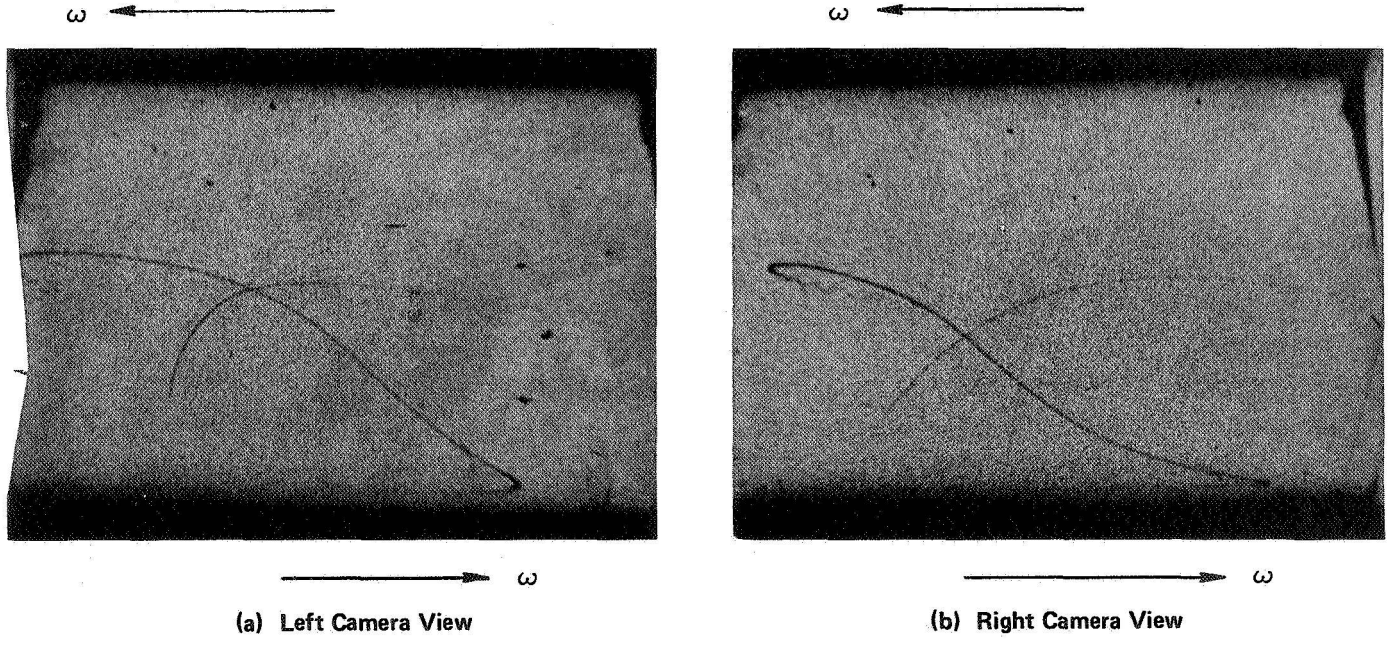

(a) Left Camera View

(b) Right Camera View

FIGURE 3.16 STEREOPAIR VIEWS OF PARTICLE PATHLINES IN THE FLOAT ZONE MODEL WHEN COUNTER-ROTATING AT ω = 1.25 REV/SEC USING A VERY DILUTE PARTICLE SOLUTION

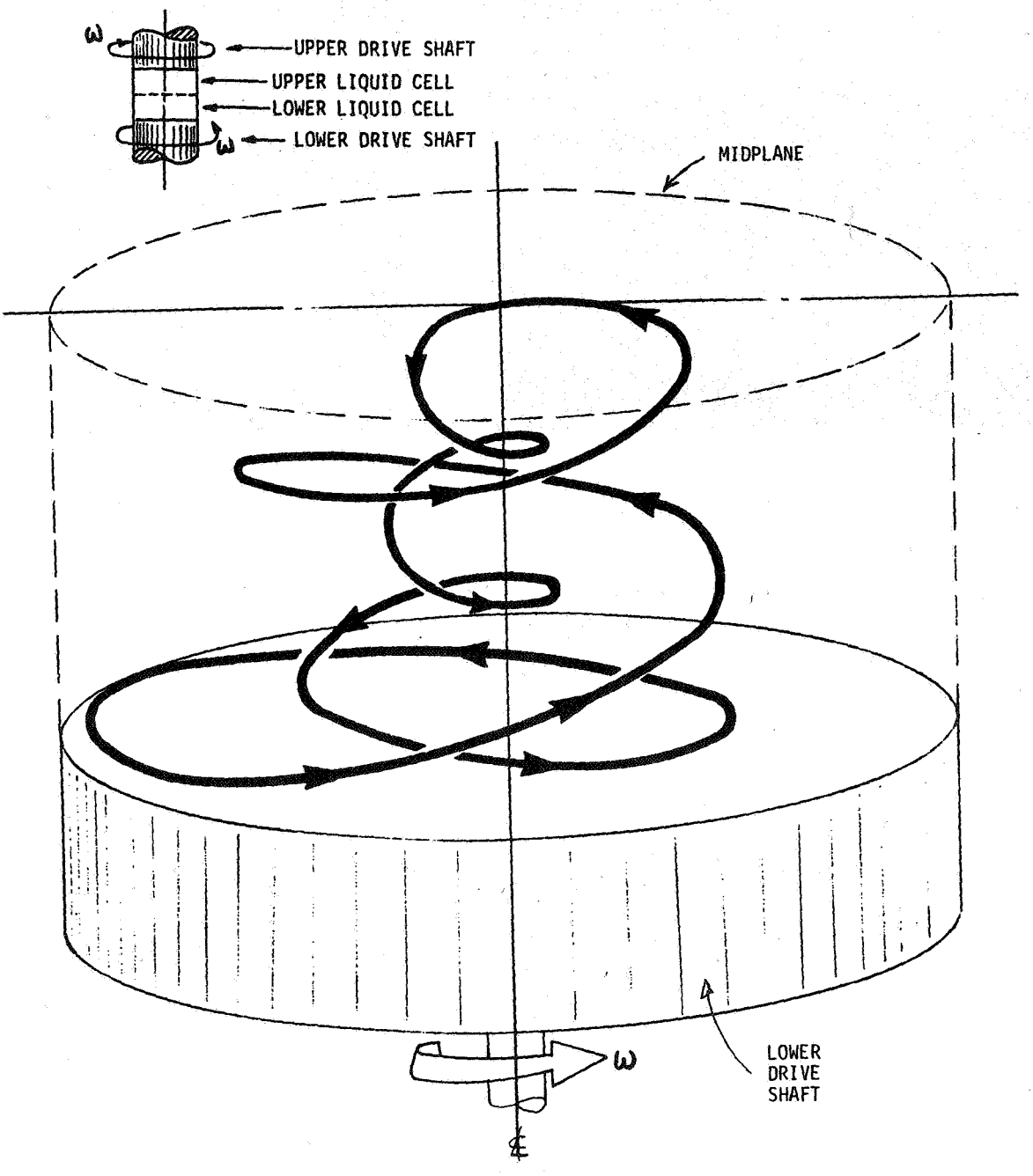

FIGURE 3.17 APPROXIMATE PATHLINE IN LOWER ROTATING WATER CELL, AS SEEN BY STATIONARY OBSERVER. UPPER CELL OF EQUAL DIAMETER ROTATED AT EQUAL RATE IN OPPOSITE SENSE. SKETCH SHOWN FOR ABOUT 6 SHAFT ROTATIONS AT ABOUT 1 REV/SEC. CELL APPROX. 5 mm DIA. x 2 mm HIGH. NUMBER AND DIAMETER OF SPIRALS DEPENDENT ON ROTATIONAL RATE AND PARTICLE LOCATION.

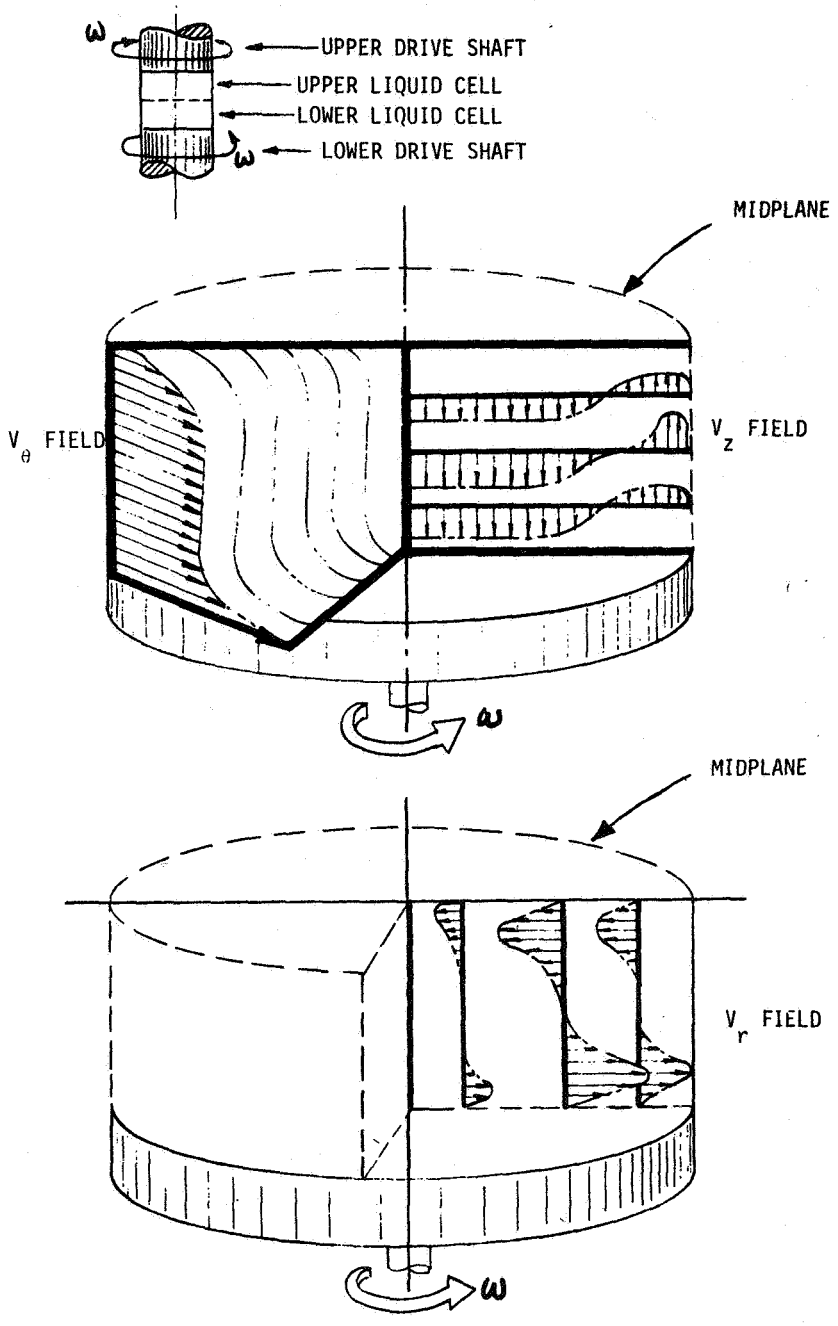

FIGURE 3.18 ESTIMATED VELOCITY DISTRIBUTION IN LOWER ROTATING LIQUID CELL FOR EQUAL DIAMETER, COUNTER-ROTATING DRIVE SHAFTS

4.0. ECONOMIC IMPACT ANALYSIS

4.1. SCOPE

Although not called for by our current contract, we have re-estimated the economic impact on the electronics industry of producing crystal silicon (Si) in space by the float zone process for eventual use as a substrate for electronic devices.

We have updated the economic impact estimates published in our Interim Report, "Float-Zone Processing in a Weightless Environment", October 1974, (Contract No. NAS8-29877) in order to provide a better basis for guiding future work. To this purpose, we seek answers to the questions:

- Should the value of our work on the float-zone processing of Si be based on the possible economic advantage of producing larger wafers in space than possible on Earth?

- Or, is the greater significance of our work related to a contribution to the better understanding of the physical processes involved in crystal growth - by the float-zone process or by any other competitive method?

Our updated estimate of economic impact has its foundations in work reported in the Interim Report previously cited. In this revision we have included the impact of the cost of space transportation on the economics previously developed. Also, the time frame for possible space processing and the competition between Czochralski and float-zone processed Si crystal has been given more consideration.

As a basis for evaluation, we have assumed transportation costs in the range of $100/kg to $1000/kg. The former figure is consentient with the expectations of transport costs using a heavy lift launch vehicle (HLLV) planned for service early in the twenty-first century. The latter figure is in agreement with the expected cost of transportation using the Shuttle. As an index of economic impact, we have estimated the maximum potential savings accruing to the U.S. electronics industry as a result of the float zone processing of crystalline Si in space during the decade 1995 to 2005.

4.2. RESULTS

Appendix C provides all results and the methods and assumptions used to estimate economic impact * are presented in detail. For convenience, the basis of these results and the assumptions critical to their interpretation are gathered here. They are:

- The float-zone production of single crystal silicon in space is to be used by the electronics industry on Earth and therefore must compete economically with that produced on Earth by whatever method.

- Possible benefits of processing single crystal Si in space as a research endeavour or the possible benefits of producing crystals in space for space use is not considered.

- Production of single crystal silicon by the ribbon process has not been examined.

- Nothing fundamental prevents crystal silicon wafer of the most economic size from being produced by the Czrochralski or modified float-zone method on Earth or in space by 1995.

- The costs of capitalization, energy, and labor are the same in space as on Earth.

- No special value has been placed on Si crystal of superior quality nor on the possibility of reduced energy payback (reflected at Earth) by utilization of the Sun as a source.

- The economics and technology of today relative to Si crystal growth processes will persist to the year 2000.

---

* In subsequent discussion of economic impact, our use of the word "cost" refers to the cost to the buyer or the seller's "price". We use the word "value" in reference to the costs associated with the final stages of processing a Si wafer into a useful device. The value added due to final processing of a bare, polished wafer to a final device is assumed to be 100 percent of the added price of the final device resulting from this process. The value added has significance in respect to the size of wafer entering the final process. The assumption of 100% value added gives maximum credit to the value of larger wafers. The subtlety of these definitions are not very important. They have little significance compared to other uncertainties of our evaluations.

Subject to these qualifications, Figures 4.1, 4.2 and 4.3 summarize results basic to our subsequent estimates of overall economic impact. These results are plots of the calculations appearing in Tables C.3, C.4 and C.5 of Appendix C. From these figures we note the following:

- If comparisons are made between different size wafers, there is almost no economic advantage, for most wafer sizes there is a disadvantage, if the transportation costs are $1000/kg.

- For a transportation cost of $100/kg, there is a range of larger crystal wafer sizes where a space-based production has economic advantage, if it is presumed this range can be produced in space and not on Earth.

- This possible cost advantage due to wafer size increases with the complexity of the device which uses crystalline silicon as a substrate.

Figures 4.1, 4.2 and 4.3 indicate a potential economic value for crystal silicon substrates processed in space by the float zone process from wafers of larger size. If we assume that the largest wafer possible to produce on Earth by the float zone process has a 3 inch diameter and larger wafers are possible to make in space by the same technology, we note that the maximum economic benefit (expressed by the ratio of the cost of crystal silicon substrate per unit area resulting from a space process to that resulting from an Earth process) is in a range of 0.89 to 0.35, depending on the complexity of the final electronic device, for a transportation cost of $100/kg. These ratios derive from comparing the magnitudes of the cost shown as large dots in Figures 1 through 3. Stated in slightly different terms, we find that the maximum potential savings to the electronic industry, expressed as a fraction (one minus the cost ratio) resulting from float-zone, space-processed silicon wafers is in the range of 0.11 to 0.65. The distribution of potential saving among the electronic devices that currently make up the market is shown in Figure 4.4.

Our final index of the economic impact of float-zone crystalline Si produced in space is based on that portion of a future market that can possibly be commanded by the product. In this evaluation we have made estimates based on the following assumptions:

- The total cumulative market for Si wafers in the decade 1995 to 2005 will be that arrived at by an average growth rate of 10%, or about 30 million dollars.

- Of this total, about 60% or 18 billion dollars' worth, will be processed into finished electronic devices where wafer size has a potential advantage.

- The total market for crystalline Si wafers as distributed by their use in final electronic devices will be the same in the year 2000 as it is now; that is, about 17% in Si diodes or rectifiers or solar cells, 31% in transistors or thyristors, 20% in MOS or IC, and the remaining 32% in bipolar IC.

- Within these market subdivisions, Si wafers processed by the float-zone process will retain their current share. This assumption argues that nothing fundamental prevents crystal silicon wafers produced by the Czrochralski method (which production now dominates the market" or modified float-zone method from producing wafers of any size, on Earth or in space, nor will higher quality crystal now provided by the float-zone process have any greater market impact than at present. We estimate that float-zone produced wafers now have about 2, 5, 3 and 1% of the volume in the market segments listed immediately above.

Combining the estimate of total market value of crystal Si in the decade following 1995, the estimate of the share of this market to be realized by float-zone processed material, and the fractional savings possible in a spectrum of application (Figure 4.4), we project a total maximum economic impact of 237 million dollars - as represented by the savings possible to the U.S. electronics industry. This figure represents about 1.3% of the estimated comulative value of the crystal Si product under consideration.

4.3 CONCLUSIONS

From this recent work we conclude that some new technology affecting the market must develop in order to realize a clear economic advantage resulting from the production of crystal Si in space by the float-zone process. There is virtually no possible advantage until the costs of space transportation reduces to levels below that projected for the Shuttle. This fact delays possible advantage to a time when cheaper space transportation is available. For an assumed cost of transportation equal to $100/kg (which is the objective of a heavy-lift launch vehicle (HLLV) planned for the period 1995 to 2005), and making all assumptions in favor of a space process, we find some possible cost advantages attendant to producing larger polished wafers in space than possible on Earth. We have estimated that the maximum possible benefits of space processing of crystal silicon represent a cumulative savings to the U.S. electronics industry in the decade 1995 to 2005 of about 237 million dollars, or approximately 1.3% of the total market value of crystalline Si processed in this decade. The reader will undoubtedly appreciate the fragility of an estimate of a 1.3% benefit when considering the uncertainties involved in the assumptions leading to this result.

Accordingly, we believe future work along the lines we have pursued has most potential benefit in the development of a better understanding of the physical processes at work in producing crystals from a melt by the most appropriate Earth-based or space-based process. This understanding can lead to the production of superior quality crystals on Earth and can provide a guide to producing crystals in space of a quality unobtainable on Earth because the detrimental effects of gravity induced natural convections in the melt can be avoided. Finally, it appears to us that the space processing of crystalline material has its greatest potential economic benefit when applied to materials having a high value, measured in dollars per unit mass (thus reducing the effect of the cost of transportation) and, in addition, having considerable additional value for having few crystal defects and a uniform and specified composition - which quality may only be possible to produce in the low gravity of a space manufacturing site. In this connection, we note that the market of superior quality crystals is a small fraction of the total market and it would have to bear the cost burden of development and capitalization of a space process. This cost should be accounted for in an economic evaluation of the value of superior quality crystals made in space. This work has not addressed the question of the value of superior quality crystals.

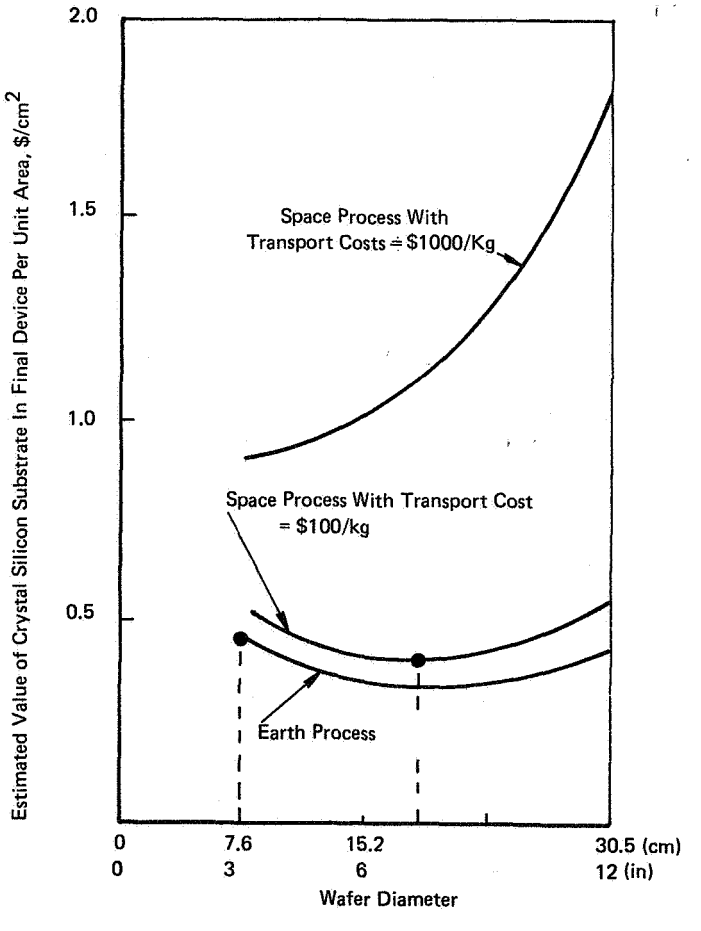

FIGURE 4.1 ESTIMATED VALUE OF SINGLE CRYSTAL SILICON SUBSTRATE FOR SOLAR CELL OR RECTIFIER

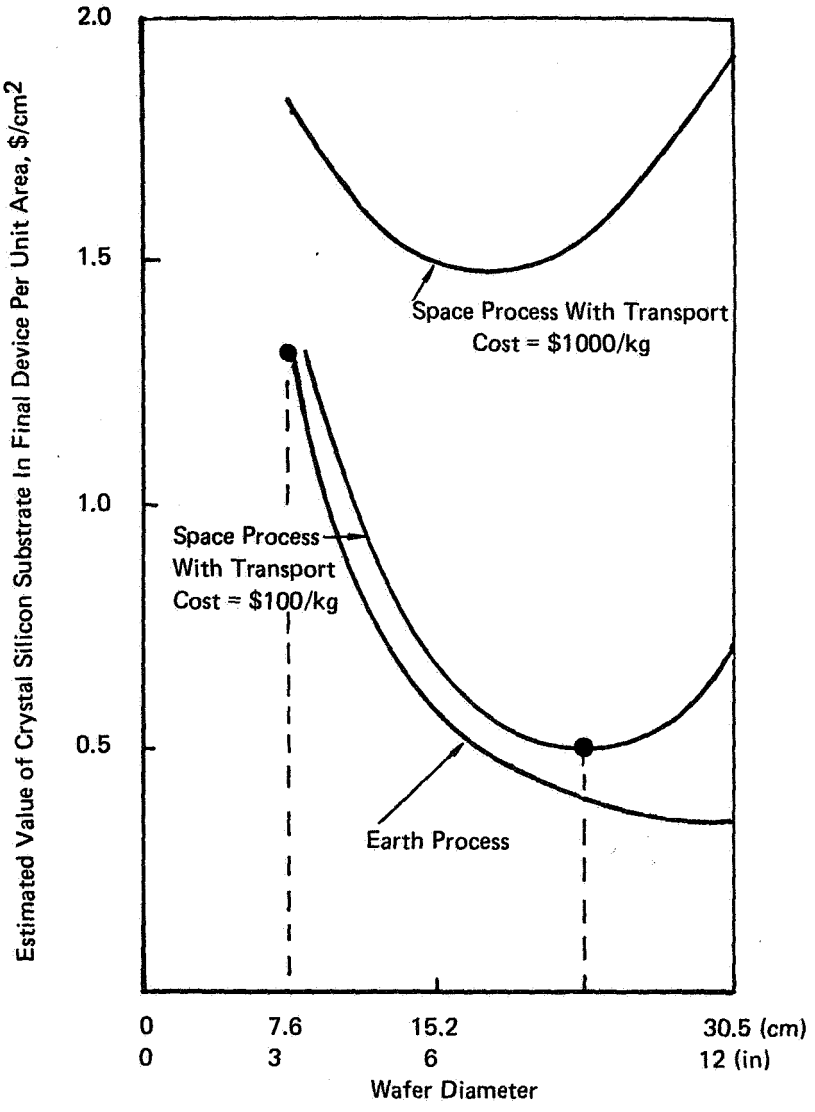

FIGURE 4.2 ESTIMATED VALUE OF SINGLE CRYSTAL SILICON SUBSTRATE FOR MOS OR IC

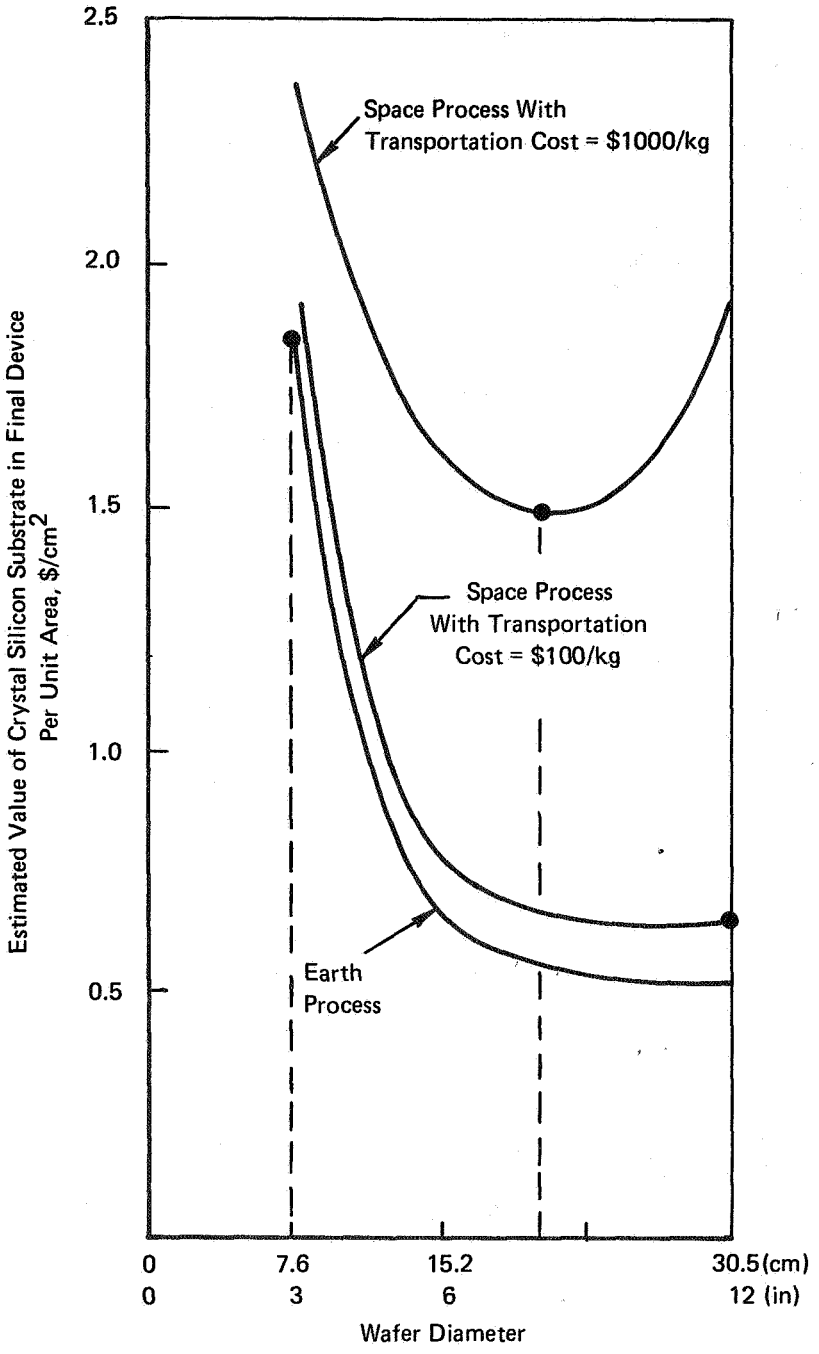

FIGURE 4.3 ESTIMATED VALUE OF SINGLE CRYSTAL SILICON SUBSTRATE FOR BIPOLAR IC

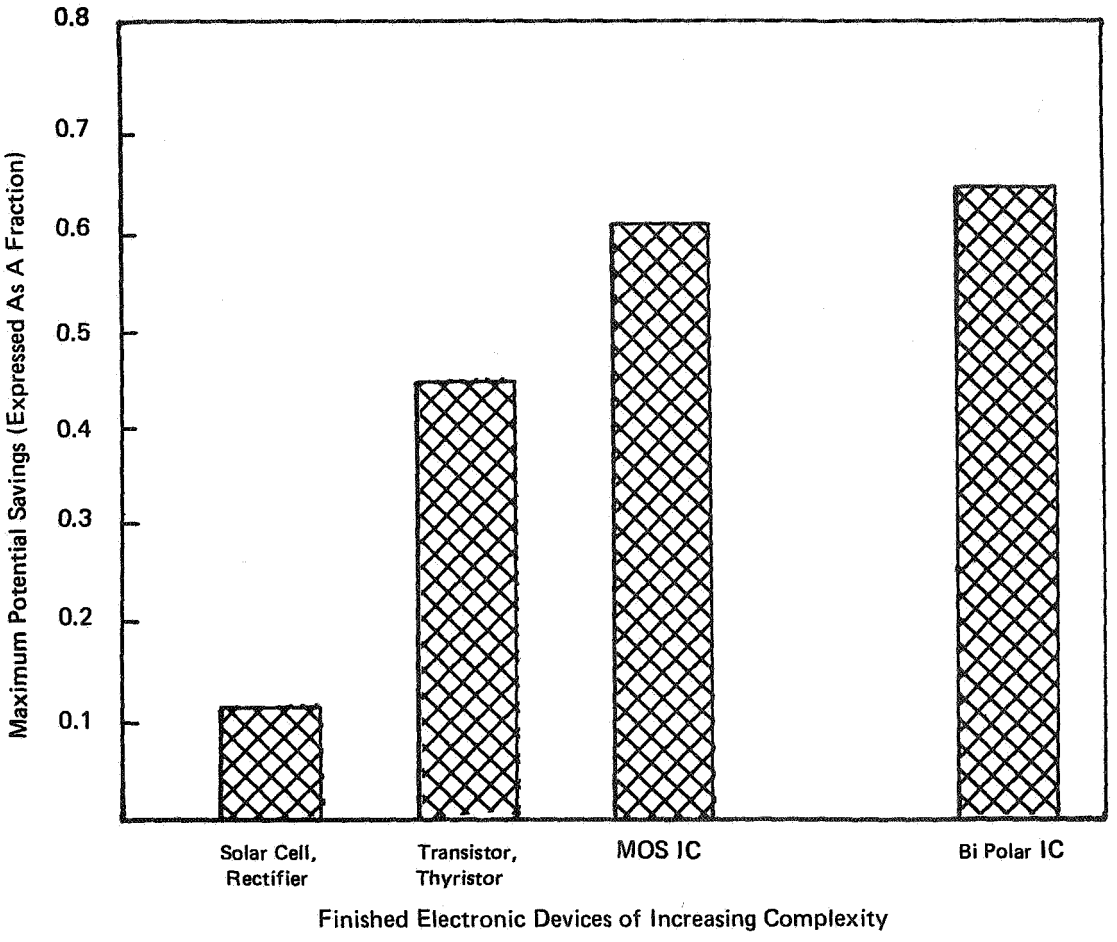

FIGURE 4.4 MAXIMUM POTENTIAL SAVINGS TO ELECTRONICS INDUSTRY RESULTING FROM FLOAT ZONE PROCESSING OF S_i IN SPACE VS. THAT PRODUCED ON EARTH

5.0 FUTURE WORK

5.1. BACKGROUND

During the two and a half year period since the inception of our work, we have witnessed a remarkable growth in the quantity and dimensions of float-zone silicon single crystals. At that time 5.1 cm (2 inch) diameter float-zone wafers were available in small quantities at a premium price. Now large quantities of 7.6 cm (3 inch) and some 10.2 cm (4 inch) diameter float-zone wafers are commercially available at essentially the same price as Czochralski wafers. There is evidence that 12.7 cm (5 inch) and 15.2 cm (6 inch) diameter crystals are being grown by the float-zone process experimentally. Based on past experience, there is every reason to believe that float-zone grown wafers will continue to approach the dimensions and cost of Czochralski wafers.

The increase in dimensions that has been realized in the float-zone process has been made possible by a major departure from conventional float-zone practice. In conventional float-zone crystal growth processes the axes of the feed stock and grown crystal are colinear and their diameters are approximately equal. With this conventional geometry, the maximum diameter Si crystal which can be grown in the gravity environment on the Earth's surface is approximately 5.1 cm (2 inch). With larger diameters the hydrostatic pressure of realizable zone heights exceeds the surface tension pressure. The larger diameters have been achieved by rotating the growing crystal and substantially smaller diameter feed rod about different parallel axes. By this means, a very thin melt zone is created which is stable at the large diameters. This highly distorted float-zone process has its origin in processes called pedestal growth techniques and might be viewed as a Verneuil process which uses a solid feed rather than conventional powder feeds.

There are several important consequences of growing single crystals by this modification of the float-zone process. An axis of thermal symmetry no longer exists which means that the growing crystal is subjected to a cyclic temperature variation as it is rotated. The fluid flow patterns in the melt zone are highly irregular and may be time variant. In the region between the small diameter rotating feed and the larger diameter growing crystal, the surface velocities range from parallel to counter flow including a zero velocity singularity. The remainder of the melt is not subject to the forced convection but each point is brought into the "mixer" with each rotation of the growing crystal. This irregular flow pattern effects the bulk compositional uniformity and the boundry layer characteristics adjacent to the growing crystal in a complex and poorly understood manner.

Despite the dramatic accomplishments of the float-zone process in achieving large diameters and low costs, we anticipate that the modified growth conditions which have been developed will cause intrinsic defects which will offset the advantage of purity that float-zone crystals have. To our

knowledge, there has been no thorough study of the defects which are characteristic of crystals grown by this modified float-zone process. It is the uncertainty about the quality of crystals grown by this modified float-zone process on Earth relative to the potential quality of crystals grown by other processes on Earth or in the low gravity environment in space that forms the basis of our proposal for continued work.

We have come to the conclusion that there is only a tenuous economic value in increasing crystal diameters beyond the 10.2 cm (4 inch) to 15.2 cm (6 inch) range which are either currently available or will be shortly. Moreover, there is no obvious reason why crystals having diameters greater than 15.24 cm (6 inch) cannot be produced on Earth at some future time. The real advantage, if any, in space grown crystal will be found in quality. We believe that there are several reasons why crystals grown under proper conditions in a zero gravity environment should be superior to those grown on Earth. We believe that we can distinguish between the defect characteristics found in crystals produced by the highly distorted float-zone process and those grown in zero gravity by much more ideal conditions. It is important to project ultimate crystal quality so that the questions can be answered as to whether single crystal growth in space has a sound basis and, if so, which process should be used. The actual answer to these questions is complex since there are many factors to deal with, including the requisite quality for the end use of the wafers, whether it be in space or back on Earth. This set of decisions cannot be made intelligently without some knowledge of the differences in quality.

5.2 PROGRAM PLAN

5.2.1. Outline

We plan to develop this projection of quality from several considerations. We will extend the flow visualization studies both to the distorted float-zone process and to a broader range of conditions for the conventional float-zone geometry. We will subject Si single crystals grown by the distorted float-zone process to extensive characterization so that defect levels can be catalogued and correlated with operational features of the growth process. The flow visualization and defect characterization analyses would form the basis for our projecting probable crystal quality with the improvement of the process or its use in a zero-gravity environment. We will also model the growth of large silicon single crystals in zero gravity by a conventional float-zone technique as has been analyzed in our previous work. This modeling will consist of growing silicon single crystals with dimensions and under conditions selected to minimize natural convective effects in comparison to other determinants of crystal growth. These crystals will be characterized for comparison with those grown by the distorted float-zone process presently used for large diameter Si crystals. We will attempt to project the effect of surface tension driven convection based on direct experimental observations. Each of these activities is discussed in more detail below.

5.2.2. Flow Visualization Studies

We propose to make additional flow visualization studies using slightly modified versions of the apparatus described in this report. Two basic float-zone geometries would be modeled: the conventional, colinear crystal and feed stock arrangement and the parallel but off-axis growth arrangement now used to produce the largest diameter single crystal Si by the float-zone method. For both geometries we would expect to model the molten zone with water and use tracer particles as these techniques have proved satisfactory. Moreover, for both geometries, we would scale the smaller diameter (feed stock) to 0.5 cm. The larger diameter (crystal) for the parallel, off-axis growth method would be more than twice as large.

We would expect to increase the range of flow velocities that can be tracked by photographic means by increasing the reflectivity of the tracer particles by coating them with nickel as described in Appendix A. We would also supplement the photographic system with appropriate high-speed movie cameras. Analytical work necessary to support the intent of these experiments and to interpret results would be included. The essential nature of these analyses would be in the area of fluid mechanics.

5.2.3. Surface Tension Driven Flow Study

We propose an experiment whose purpose is to help solve the uncertainties surrounding the influence of surface tension driven flows on crystal growth. In order to do this we propose to model the system used as a basis for the analytical work of Chang and Wilcox.[2] This model consists of a cylindrical, heated molten zone having a height equal to its diameter. No forced convection is induced (no rotation) and no gravity is present, the latter eliminating natural convection effects. Reasoning based on dimensional analysis predicts that a model of this situation can be achieved on Earth at small geometric scale (a model zone diameter and height of 0.5 cm may be appropriate).

We would intend to construct this model using an improved flow visualization apparatus and techniques developed to date. A single hot-wire, circular ring placed around and coaxial with the model melt at its mid-plane would provide the heat source. The molten zone may best be modeled by n-tetradecane (C_{14} H_{30}) or its near relatives. This fluid is substituted for water because it obviates serious problems due to the effects on surface tension of thin films of organic materials adhering to the model freezing and melting interfaces should water be used. It is also relatively non-volatile and transparent. Appropriate differential temperatures on the exposed surface of the model molten zone would be measured, probably using thermistors. The nature of the flow patterns and the magnitude of the velocities induced by surface tension would be observed and measured. These observations and measurements would be compared to the predictions of Chang and Wilcox and interpreted in terms of the importance of surface tension to space-processed single crystal.

5.2.4. Simulation of Zero-Gravity Crystal Growth Using a Small Scale Si Process

As another element in the overall development plan, we propose to simulate the growth of large diameter Si single crystals in zero gravity by a floating zone process with conventional geometry. We will accomplish this simulation by operating under model conditions where the surface tension driven convection forces should dominate buoyancy induced convection as would be the case in zero gravity. Our analysis of these forces in Si indicates that surface tension driven convection should exceed that driven by buoyancy effects by one order of magnitude for zone heights and zone diameters less than 0.34 cm.

Crystals will be grown under varied growth conditions and characterized. The growth conditions will be adjusted to maximize crystal quality under model conditions which are realizable in large diameter crystals. For instance, it is probable that steeper axial temperature gradients can be achieved across a flat solidification interface in small crystals than is the case with large crystals. Thus, it is important that the modeling be done carefully to insure the validity of projections about the quality of crystals grown in a near-zero gravity environment.

The melt zones will be heated by laser and direct coupled rf means. The laser is especially useful for growing small diameter crystals and also simulates the heat flux generated by a solar heating means which may be used in space. Rf heating permits the heat to be generated within the bulk of the melt rather than on the exterior surface as is the case with laser heating.

These crystals and the large diameter crystals grown commercially by the distorted float-zone process will be subjected to the same characterization techniques. In this way we would hope to identify the relative perfection of large crystals grown in space by the conventional float-zone arrangement with large crystal grown on Earth by the distorted, float-zone method. Analytical work necessary to provide a sound foundation for this experimental program and to interpret its results would be included as an essential element.

5.2.5. Other Zero-Gravity Experiments

Based on the results of the programs previously described we would devise experiments which would use zero-gravity airplane and/or rocket trajectories and Shuttle capabilities to best advantage.

APPENDIX A

PHOTOGRAPHIC TEST SYSTEM DESIGN

A.1. INTRODUCTION

In order to obtain qualitative and quantitative information regarding the flow of fluid in the model of the molten zone, we inject a number of small spherical particles into the zone. These are illuminated by a dark field system and, since the particles follow the streamlines, the hydrodynamic flow is made visible. By using stereoscopic flash photography, we are able to make quantitative measurements of the velocity vector at various positions in the zone. In this section we analyze the photographic and illumination systems from a theoretical point of view in order to determine the F-number and magnification to be used in the camera and the light energy needed for exposure.

A.2. OPTICAL DESIGN CONSIDERATIONS

When we look at the cylindrical column of water from a distance we gather, with one eye, nearly parallel rays of light that have emerged from the surface of the water column. In order to interpret our observations therefore, it is interesting to determine what rays inside the liquid give rise to the emergent rays or, what is the same thing, the ray paths followed by parallel rays of light incident on the cylinder.

In Figure A.1 we show the effect of the refraction at the front surface only of the water column. In the front semicircular region it is true that the rays are mostly not too far from being parallel to each other, and we can therefore rely on our vision to give us a fairly undistorted view of the behavior of the flow in this region.

In the rear semicircular region, however, the picture is much more confusing. The most conspicuous feature of this region is the presence of a shadow zone. Particles in this zone will be invisible to us, and, worse still, the very existence of the shadow zone will not manifest to the observer at all: for rays emitted by objects in the protofocal or euphotic zone or near the caustic will emerge near the edge of the cylinder so as to give the impression that we have the contents of the entire cylinder in view. Objects in the euphotic zone will be greatly enlarged, but astigmatically, so their position along the horizontal direction will be confused. This, or course, implies that a stereoscopic observation will not yield precise information regarding their position in the horizontal plane. Also, because of refraction, an object will appear to be brighter when it is in the rear region than when it is in the front region.

We now consider some of the theoretical aspects of photographing a small particle in dark field illumination. As the presence of the water column does not have much effect on the view of particles near the front, but complicates the theory needlessly, we will treat the problem as though the particle were in air. The spherical particles we consider are smooth, small, and illuminated by light coming from one direction, which we treat as though it consisted of plane waves. We assume the light to be scattered isotropically by the spherical particle, so that all we see at a distance is a tiny glint which acts essentially as a point source, much like a star in the sky. The camera lens will not produce a detailed image of the glint but simply a diffraction pattern, much after the manner of an astronomical telescope. In the absence of other information, we will assume that the diffraction pattern is the classical Airy disc, even though this may not be a very good approximation at large apertures. Note that we are not concerned with behavior of the lens for rays that are much off the optic axis. Figure A.2 illustrates the photographic system in schematic form.

For our purposes we consider the camera to consist of a lens of focal length f and a photographic emulsion placed at a suitable distance, x_2 behind the lens. The plane in the object that is in sharpest focus is at a distance x_1 in front of the lens; the quantity x_1 satisfies the lens formula

$$\frac{1}{x} + \frac{1}{x_2} = \frac{1}{f} \tag{A.1}$$

The object occupies a finite region between planes situated at distances $x_1 + \Delta x_1$ and $x_1 - \Delta x_1$ in front of the lens; x_1 is half the depth of field. We define the magnification M to be

$$M = \frac{x_2}{x_1} \tag{A.2}$$

and characterize the aperture of the lens by the number

$$F = \frac{f}{D} \tag{A.3}$$

where D is the diameter of the aperture.

A point of light in the plane at distance x_1 in front of the lens will be imaged as a bright circle surrounded by fainter rings (the celebrated Airy pattern). The diameter of the central disk is

$$D_a = 2.44\ \lambda F \tag{A.4}$$

where λ is the wavelength of light employed. The diameter of the blur circle (calculated by geometrical optics) for objects focused at a distance $x_2 \pm \Delta x_2$ behind the lens is

$$D_b = \frac{|\Delta x_2|}{F} = \frac{M^2}{F} |\Delta x_1| \tag{A.5}$$

The depth of field may be set by letting $D_b = D_a$*. Thus

$$|\Delta x_1| = 2.44 \lambda \left(\frac{F}{M}\right)^2 \tag{A.6}$$

The diameter of the resolution element, Δy_1, in the object plane is found by dividing the diameter of the resolution element at the image plane by the magnification M, thus:

$$\Delta y_1 = \text{larger of } \frac{D_a}{M} \text{ and } \frac{\varepsilon_f}{M} \tag{A.7}$$*

where ε_f = diameter of resolution element of the photographic film employed. In the present case we can easily arrange to have

$$D_a \geq \varepsilon_f, \text{ so we use}$$

$$\Delta y_1 = \frac{D_a}{M} = 2.44 \lambda \left(\frac{F}{M}\right) \tag{A.8}$$

Equations A.6 and A.8 show that the depth of field and the size of the resolution element in the object depend only on the ratio F/M (for light of a given wavelength). We would like Δy_1 to be small (high resolution) and $|\Delta x_1|$ to be large (large depth of field), but these are conflicting requirements.

As an example of a reasonably good arrangement, let $|\Delta x_1| = 0.25/1.33$ cm (we are taking advantage here of the index of refraction of the water)

$$\lambda = 560 \text{ nm}$$

whence F/M = 37.1

and $\Delta y_1 = 50.7$ μm

---

* The depth of field can also be computed from the theory of diffraction. The quantity 2.44 in Equation A.6 corresponds to a Strehl ratio of 0.73.

Now assume $\varepsilon_f = \frac{1}{150}$ mm

and let $D_a = 2\varepsilon_f$ (this will avoid excessive graininess in the picture)

Then, from Equation A.4,

$$F - 9.76$$

and therefore M - 0.263.

If the subject is 0.5 mm wide, we find the number of resolution elements it spans is

$$n_e = 98.7$$

which will enable us to resolve the details of the flow well enough for the present purposes.

Of course, it must be realized that some of the assumptions that enter this calculation are quite arbitrary. In practice, we preferred to employ higher magnification (0.5 to 0.7) at the expense of increasing the size of the blur circle produced by particles out of the plane of best focus. The principal advantage of this is to reduce the difficulty of enlarging the negatives, a consideration not treated theoretically here. Even with M = .5, however, enlargement of about 35x were required for useful prints and had to be made in our microscopy laboratory.

We now consider the problem of illuminating the spherical particles to enable them to be photographed. In order to make quantitative measurement of the velocity vector possible, we decided to use three unequally spaced flashes of light to make the photographs, and to record the images on two cameras simultaneously, placed so as to produce stereo pairs. By this means it should be possible to determine the magnitude and direction of the velocity of the particle. Note that if only two flashes were used, the magnitude of velocity could be determined but the direction would be determined ambiguously with respect to sign.

At this point, therefore, we must calculate the energy, W_0, needed in the flash (produced by an Xenon flash tube) to make one exposure of the film. The arrangement of the elements of interest is sketched in Figure A.2.

To start, we assume that the source releases an amount of energy, W_0, in one flash. A fraction $\Omega_0/4\pi$, of this energy falls on the condensing lens which concentrates the light to give an energy density W''_p, in the vicinity of the particle in the water column of radius b, as follows:

$$W''_p = W_0 \frac{\Omega_0}{4\pi} \frac{1}{\pi b^2} \tag{A.9}$$

The energy, W_s, scattered (isotropically, we assume) by the particle of radius a and reflectivity R_p is a fraction of the incident energy and is given by the expression

$$W_s = \pi a^2 R_p W''_p \tag{A.10}$$

Of this a fraction, $\Omega_1/4\pi$, falls on the camera lens and is concentrated into a focus of radius $1.22 \lambda F$.

Therefore, the energy density at the focus is

$$W''_f = \frac{\Omega_1}{4\pi} W_s \frac{1}{\pi(1.22 \lambda F)^2} \tag{A.11}$$

In Equations A.9 and A.11 Ω_0 and Ω_1 are solid angles of the acceptance cones of the condenser and camera lenses, respectively, which are related to the half-angles θ_0 and θ_1, of the cones by the relations

$$\Omega_0 = 2\pi(1-\cos\theta_0) \tag{A.12}$$

$$\Omega_1 = 2\pi(1 - \cos\theta_1)$$

We find furthermore, if F_0 is the F-number of the acceptance cone of the condenser, that

$$\tan\theta_0 = \frac{1}{2 F_0} \tag{A.14}$$

$$\text{also } \tan\theta_1 = \frac{M}{2F} \tag{A.15}$$

Upon combining Equations A.0 through A.13 we find

$$W_0 = \frac{4\pi b^2 (1.22 \lambda F)^2 W''_f}{R_p (1-\cos(\theta_0)(1-\cos\theta_1) a^2} \tag{A.16}$$

to be the energy needed in the source in order to give an exposure W''_f to the photographic emulsion. For a Xenon flashlamp and a slow panchromatic emulsion, W''_f is given by Altman et al [5] as

$$\frac{10^{-7}}{6.7} J.cm^{-2}.$$

If we also take

$a = 2\ \mu m$

$b = 0.25\ cm$

$F = 10$

$F_0 = 2$

$M = 0.5$

$$R_p = \left(\frac{n_p - n_w}{n_p + n_w}\right)^2 = 0.0036$$

where

n_p = index of refraction of particle = 1.5 (clear glass or plastic)

n_w = index of refraction of water = 1.33

$\lambda = 560\ nm$

we find

$W_0 = 4.07\ J$

which is within the capability of a small Xenon flash tube. A medium speed pan film requires only about 1/4 the energy density of a slow pan film.

The calculation given above indicates that it is feasible to make flash pictures of the type envisaged. It also indicates that there is great room for improvement in the reflectivity, R_p, of the scattering particle, which is low because the impedance mismatch between the particle and the water is not very great. Of course, particles of larger radius than 2 μm will require less energy to cause their images to be recorded on the emulsion.

Two methods can be employed to improve the reflectivity. One is to use hollow glass spheres, for the air-glass interface has a nominal reflectance of $R_p = 0.047$. The spheres can be selected on the basis of density by letting them float or sink in various liquids. They can be separated on the basis of size by letting them fall for a certain time in a column of still air. Although we have not used such spheres in any flow experiments, we have carried out the density selection on samples of hollow glass spheres.

A second method is to plate the spheres to give them a shiny metallic surface. In this case a reflectivity of $R_p = 0.5$ or so should be relatively easy to achieve. We have experimentally plated small hollow glass spheres with electroless nickel, but these have not been selected on size nor have they been used in any flow studies. Nickel was selected as a coating material because it is fairly easy to apply and does not tarnish readily.

A.3 PHOTOGRAPHIC APPARATUS

Stereo photographs were taken with a pair of 35 mm cameras which were mounted on an aluminum plate, such that the optical axes of the cameras intersected at an angle of 30 degrees. The optical axes were also aligned to be normal to the axis of the water model of the float-zone. One camera was an Exacta and the other a Nikon. Attached to each camera was a bellows focusing attachment and a 105 millimeter focal length lens. The lenses were adjusted to provide a magnification of about 0.8. Panchromatic film with an ASA rating of 64 was used and then developed as recommended in D19 developer.

Two types of light sources were used to illuminate the spherical particles in the liquid zone: 1) a stroboscopic xenon flash was used to measure the velocity of the tracer particles and 2) an incandescent lamp was used to show the pathlines taken by these particles.

The xenon flash apparatus consisted of a modified General Radio Company, type 1531-A strobotac. By means of external circuitry, the capacitance of the discharge capacitor in the strobotac was increased from 1.15 μF to 17.15 μF at a charging potential of 800 volts. Thus, the energy in the discharge was increased to 5.48 Joules. This energy level was in conformity with that previously calculated as necessary to expose a medium speed film under the conditions stated. Although the xenon flash lamp used in the strobotac is a type FX6A, rated at a maximum level of 5 Joules, it could be operated satisfactorily during a short duty cycle at a level of 5.48 Joules.

In order to determine the velocity vectors of the particles, stroboscopic flash sequence provided by a control box attached to the Strobotac trigger input jack was used. The circuitry was designed such that a series of three trigger pulses were sent to the strobotac which produced three flashes. The three flashes were derived from a sequence of four trigger pulses which were evenly separated in time, the pulse rate being established by an external signal generator. The seond pulse was omitted from

the trigger pulse train delivered to the Strobotac. By omitting one flash, the direction of the particle could be established and from the time interval between flashes the particle speed could be computed. The operational range of the sequence flash system designed was satisfactory for signal generator frequencies ranging between 5 and 50 Hertz.

Incandescent illumination of the particles was provided by a small reflector type of tungsten-halogen lamp. A Sylvania type ELS Quartz Tru-Beam lamp was used for this purpose. The ELS lamp is rated at 50 watts at 16 volts and was operated at full voltage. Because of the high heat dissipation from this lamp, it was turned on only for a period of time necessary for a photograph in order to minimize the evaporation of water used for the model of the Si melt.

When using the xenon flash, both camera shutters were operated on the bulb setting. The shutters were both opened, then the flash sequence was triggered and the shutters were closed, thus avoiding any necessity of synchronizing the shutters with the flash sequence.

Photos made with the incandescent source were taken by setting both camera shutter mechanisms to provide exposures of 1/2, 1, 2 or more seconds and then both shutters were actuated by hand as close to the same time as possible. Because precise synchronization was unimportant to the result looked for, this method was adequate.

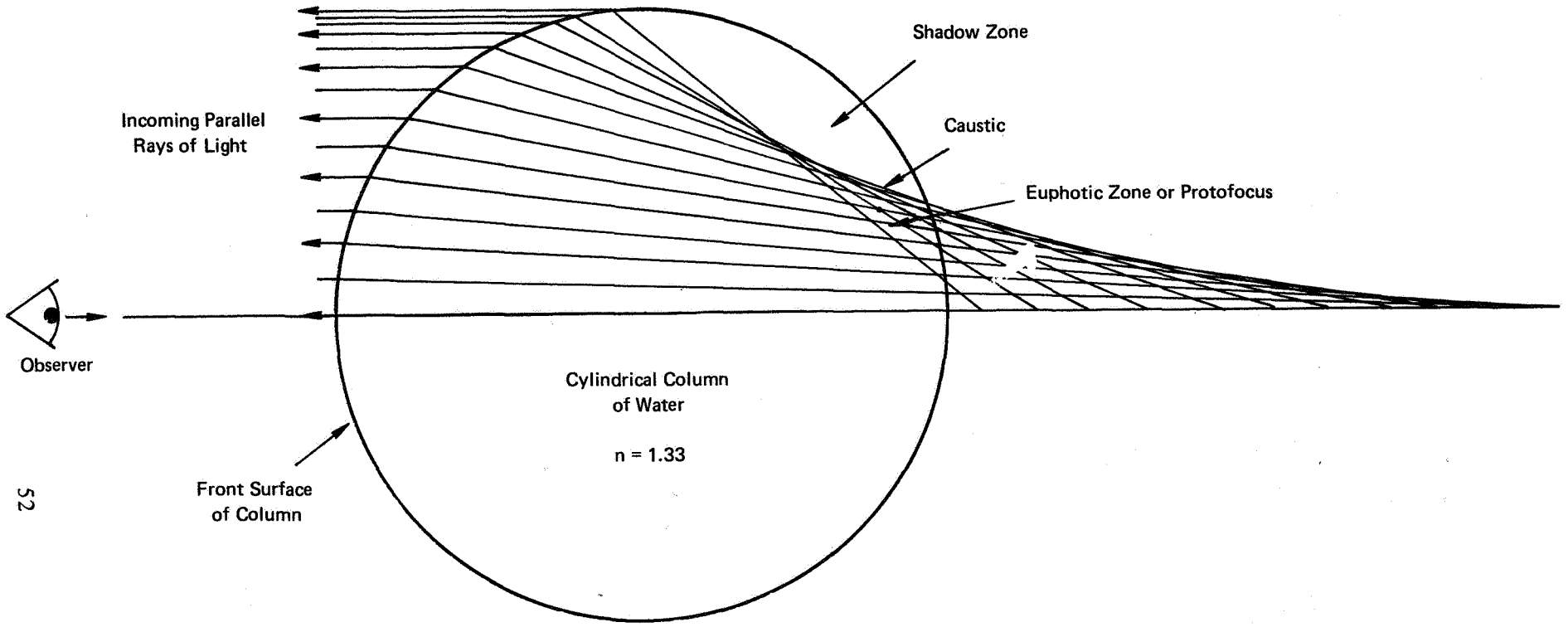

FIGURE A.1 CONSTRUCTION SHOWING THE REFRACTED RAYS OF LIGHT WITHIN A CYLINDRICAL COLUMN OF WATER

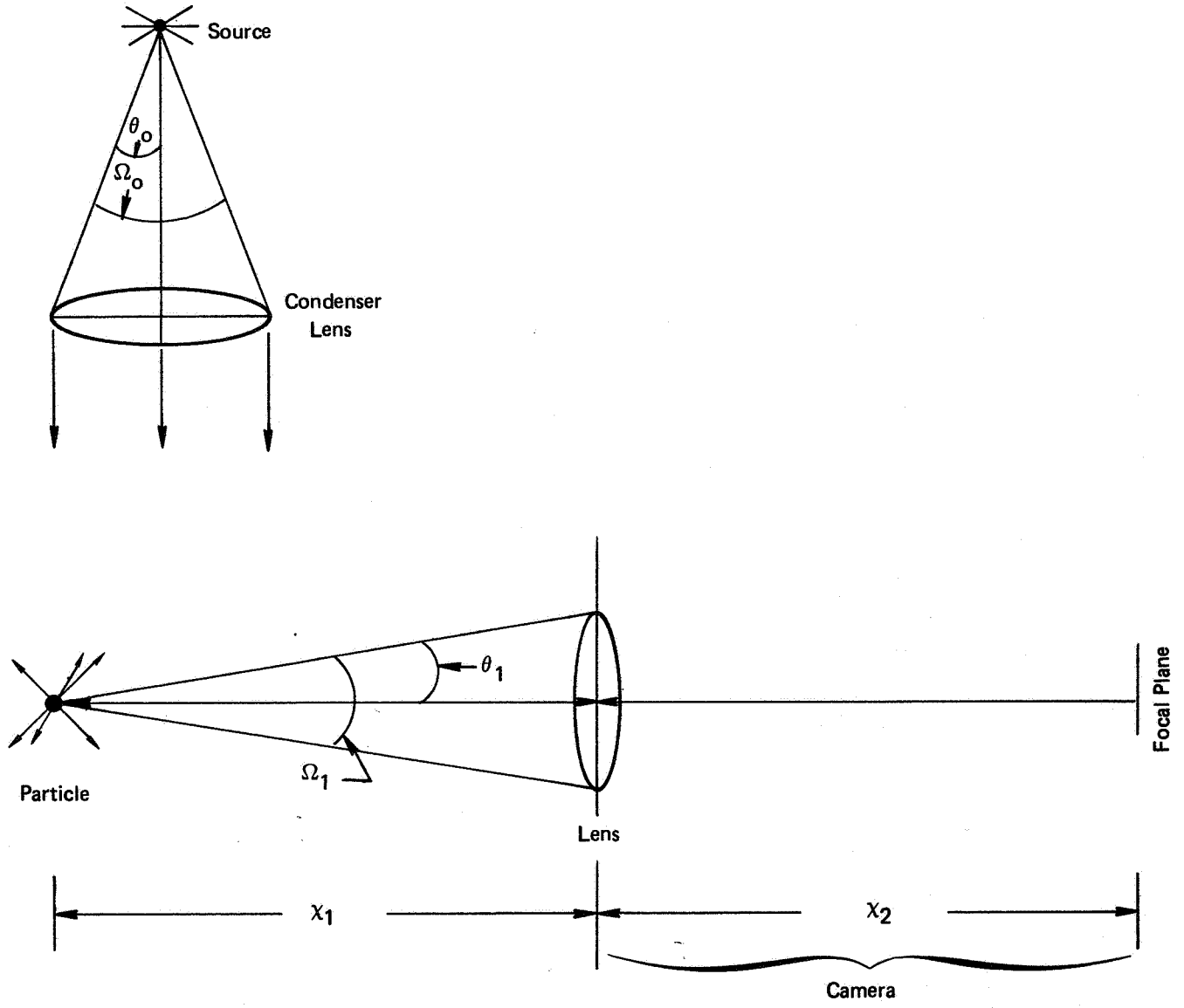

FIGURE A.2 SYSTEM TO PHOTOGRAPH A PARTICLE IN DARK FIELD ILLUMINATION

APPENDIX B

EFFECT OF GRAVITY AND LOCAL FLUID ACCELERATION ON THE ABILITY OF SMALL SPHERICAL PARTICLES TO GIVE AN ACCURATE TRACE OF THE LIQUID FLOW FIELD

B.1. GRAVITY EFFECT

The spherical particles we use to make visible the flow patterns in the liquid are, in general, of a density different from the liquid density and therefore are acted on by gravity as well as the hydrodynamic forces. In consequence, the particles will not follow the streamlines exactly, and it is our purpose in this section to estimate the magnitude of the errors involved.

The flows we are concerned with are all rotational in character, so we select as a model flow the case of solid body rotation about a horizontal axis, say the x-axis. If the z-axis is the vertical, we may describe the flow mathematically by the equations:

$$v_y = -\omega z \tag{B.1}$$

$$v_z = \omega y \tag{B.2}$$

where ω is angular velocity

v_y, v_z are y and z components of velocity.

The particle, however, has an additional vertical component of velocity, u_z, which, according to Stokes, is constant and given by the expression[6]

$$u_z = \frac{g\,(\rho_\ell - \rho_p)\,d_p^{\,2}}{18\mu_\ell}$$

where g = gravitational constant, $cm^2 - s^{-1}$

ρ_ℓ = density of liquid, $g - cm^{-3}$

ρ_p = density of sphere, $g - cm^{-3}$

d_p = diameter of sphere, cm

μ_ℓ = viscosity of liquid, $g - cm - s^{-1}$

Thus the equations of motion of the particle are:

$$\frac{dy}{dt} = -\omega z \tag{B.3}$$

$$\frac{dz}{dt} = \omega y + u_z \tag{B.4}$$

We solve these by differentiating Equation B.4 and substituting ωz for $\frac{dy}{dt}$, getting:

$$\frac{d^2z}{dt^2} = \omega\frac{dy}{dt} = -\omega^2 z \tag{B.5}$$

Suppose the particle starts at a distance b from the origin at such time that

$$z = b \sin \omega t \tag{B.6}$$

is the correct solution of Equation B.5. Then from Equation B.4

$$y = \frac{1}{\omega}\frac{dz}{dt} - \frac{uz}{\omega} \tag{B.7}$$

so

$$y = b \cos\omega t - \frac{u_z}{\omega} \tag{B.8}$$

Equations B.6 and B.8 represent a circle of radius b with center at $y = -\frac{u_z}{\omega}$, while the streamline itself is a circle of radius b with center at the origin. Hence, the magnitude of the error is

$$\varepsilon = \left|\frac{u_z}{\omega}\right| = \frac{g\, d_p^{\,2}\, (\rho_\ell - \rho_p)}{18\mu_\ell \omega} \tag{B.9}$$

If this quantity is very small in comparison with the physical size of the liquid zone, the particle will accurately follow the streamline.

For example, let the fluid be water and the sphere be glass with a radius of 10 μm. We take

$$g = 980 \text{ cm}^2\text{-s}^{-1}$$

$$d_p = 2 \times 10^{-3} \text{cm}$$

$$\rho_\ell = 1 \text{ g - cm}^{-3} \quad (H_2O)$$

$$\rho_p = 2.8 \text{ g- cm}^{-3}$$

$$\mu_\ell = 0.01 \text{ g - cm}^{-1}\text{s}^{-1} \quad (H_2O)$$

$$\omega = 20\pi \text{ rad - s}^{-1} \quad (600 \text{ R.P.M.})$$

We find, from application of Equation B.9 that

$$\varepsilon = 6.24 \ \mu\text{m}$$

which is an acceptably small value in view of the fact that the diameter and height of the liquid zone are about 0.5 cm each. Moreover, the spheres finally used in flow visualizations studies were polystyrene which has a density less than that of glass used in the example.

B.2 ACCELERATION EFFECT

The characteristic time to accelerate a particle starting at rest within a flowing fluid medium of velocity V_ℓ to some specified fraction of this velocity is used as an index of the ability of the particle to follow the local streamline and, hence, be a good indicator of the flow field. Choosing values appropriate to our experimental, viz:

Set diameter of particle, $d_p = 10\mu = 10\text{x}10^{-6}\text{m} = 1\text{x}10^{-3}$ cm

Set density of particle $\rho_p \sim 1$ gm/cm^3

Set the relative velocity of the particle to the local stream velocity $(V_\ell - V_p)$ at a maximum value of 10 cm/sec

Viscosity of fluid medium, $\mu_\ell = 10^{-2}$ dyne-sec/cm^2

Density of fluid medium, $\rho_\ell = 1$ gm/cm^3

For flow in the stokes range or for $0 \leq N_R \leq 1.0$

where:

$$N_R = \text{particle Reynolds number} = \frac{\rho_\ell (V_\ell - V_p) d_p}{\mu_\ell}$$

$$N_{R|_{max}} = \frac{1 \ (10)(10^{-3})}{10^{-2}} = 1$$

the drag force, D, is equal to:

$$D = 3\pi\mu_\ell \, d_p \, (V_\ell - V_p)$$

and the particle acceleration, $\frac{d V_p}{dt}$, is equal to:

$$\frac{dV_p}{dt} = \frac{18\mu_\ell}{\rho_p \, d_p^{\,2}} \, (V_\ell - V_p) = \frac{18 \, (10^{-2})}{1 \, (10^{-6})} \, (V_\ell - V_p) = 1.8\text{x}10^5 \, (V_\ell - V_p)$$

or,

$$\int_o^{V_p} \frac{d V_p}{V_\ell - V_p} = - \ell n \left[V_\ell - V_p \right]_o^{V_p} = 1.8\text{x}10^5 \int_o^t dt = 1.8\text{x}10^5 t$$

$$\frac{V_\ell - V_p}{V_\ell} = e^{-1.8\text{x}10^5 t} \qquad \text{(B.9)}$$

From application of Equation B.9 we note that the velocity of the particle will approach within 0.1% of the velocity of the fluid medium in a time of approximately $4\text{x}10^{-5}$ sec. In this time the medium will have a local displacement of only $4\text{x}10^{-4}$ cm. Therefore, we conclude that the particles which we have used as tracers, being smaller than 10 micron diameter, will provide sufficiently accurate indication of of the fluid streamlines.

APPENDIX C

METHODS USED FOR ESTIMATING THE COST OF Si CRYSTAL PRODUCED ON EARTH AND IN SPACE

C.1. SCOPE

In this appendix we describe the methods used to estimate the comparative cost of producing finished silicon substrates (wafers, or chips) on Earth and in space by the float zone process. Moreover, because the size (diameter) of the finished wafer has a marked effect on the cost of the substrate used in the finished electronic device (rectifier, solar cell, transistor, thyristor, MOS, IC, etc.) and because larger size may be an advantage offered by space processing, the method of cost determination through this final stage is illustrated. The assumptions inherent to any particular evaluation of cost are clearly stated. The accuracy of the method with its inherent assumptions is tested by comparing the costs derived by the method outlined with the actual costs (prices)* of processed silicon wafers currently produced.

C.2. METHODS

The methods consider the costs associated with each step in the process of manufacturing a single crystal Si substrate for a finished electronic device. The final production cost of the substrate is obtained by adding the cost of each step to the cost of polycrystalline Si. These steps are: polycrystalline to trimmed single crystal boule, sawing to wafer form and subsequent lapping and polishing. Finally, the polished wafer is trimmed and processed through many masking steps involving handling, transfers, inspection and tests at a cost depending on the complexity of the final device. Because all operations up through the bare, polished wafer stage are material and energy intensive, the cost of each step is approximately proportional to the mass of Si resulting and we use the cost per unit mass ($/kg) as a scale. Therefore, the yield (defined as the mass of Si at the end of the step divided by the mass of Si entering the production step) is an important ingredient to the increment of added cost attendant to the step. Because the value added in the final stages of processing; that is, from bare, polished wafer to the fully processed substrate within the packaged electronic device is dominated by handling charges, nearly independent of wafer diameter, the cost per unit resulting useful area ($/cm^2) is chosen as an appropriate scale when considering wafers produced in different diameters.

---

*In all cases, our use of the word "cost" refers to the cost to the user, or the seller's "price".

In the case of space processed Si we consider a range of transportation costs to low earth orbit - $1000/kg appropriate to the Shuttle and $100/kg appropriate to a future heavy lift launch vehicle (HLLV).

The overall yield of the total process has particular significance with regard to the cost of space processing because the cost of transportation from earth to a space processing station is approximately proportional to the mass of material transported. Therefore, the resulting cost added to the final product due transportation charges is inversely proportional to the product of yields at each step.

C.3. BASIC CALCULATIONS

The cost of a polished Si wafer processed on Earth or in space is calculated by:

$$C_{pw} = (C_{pc} + T + C_{cc}) \div (Y_b \times Y_s \times Y_l \times Y_p) + C_s \div (Y_s \times Y_l \times Y_p)$$

$$+ C_l \div (Y_l \times Y_p) + C_p \div Y_p \qquad (C.1)$$

where

C_{pw} = cost of polished wafer, $/kg

C_{pc} = cost of polycrystalline silicon, $/kg

T = cost of transportation, $/kg ($T = 0$ for Earth processing)

C_{cc} = cost of conversion of polycrystalline Si to single crystal Si by float-zone process, $/kg

Y_b = yield of processing polycrystalline Si to a trimmed boule of crystal Si by the float-zone process

C_s = cost of sawing a trimmed boule of crystal Si into the sawed wafer product, $/kg

Y_s = yield of sawing process

C_l = cost of lapping sawed wafer, $/kg

Y_l = yield of lapping process

C_p = cost of polishing lapped wafer, $/kg

Y_p = yield of polishing process

The costs (C_c, C_s, C_l and C_p) are estimated per unit mass entering step.

The yield of the sawing process depends on the width of the saw required to cut the finished boule of crystal Si into wafers. This width is dependent on the diameter of the finished boule. Specifically:

$$Y_S = \frac{\text{wafer thickness}}{\text{wafer thickness + kerf loss due sawing}} \qquad (C.2)$$

Figure C.1 illustrates the application of equation C.1. The wafer thickness and kerf for a 7.6 cm (3 in.) diameter finished boule represents current practice. The values for a 15.2 cm (6 in.) and 30.5 cm (12 in.) diameter boule are extrapolated. From Figure C.1, we note that Y_s is about 50%, approximately independent of boule (or wafer) diameter.

We estimate the value of Y_b, Y_l and Y_p at 75%, 82% and 85%, respectively, representative of current practice. Also current practice dictates values of about \$120/kg for C_{cc}, \$175/kg for C_s, \$150/kg for C_p and C_l negligible. The current price (cost) of polycrystalline S_i (C_{pc}) is about \$65/kg. In comparing costs for Earth and space produced devices using crystal Si substrates, we chose a value of \$10/kg which is the goal or the ERDA-NASA (JPL) program to be accomplished by 1985, a date somewhat consonant with NASA's plan for possible space manufacture.

Using the above values we calculate the cost of a polished Si wafer for future Earth based process in 1976 dollars as:

$$C_{pw} = (10 + 0 + 120) \div (0.75 \times 0.50 \times 0.82 \times 0.85) + 175$$

$$(0.50 \times 0.82 \times 0.85) + 0 + 150 \div 0.85 = \$1182/kg$$

The same formula applied to current costs of polished wafers (introducing the current value of C_{pc} = \$65/kg) yields a cost of polished wafer equal to \$1393/kg.

This latter result should compare with the \$1000/kg representing the current industry price for 3 inch wafers. Several articles, published recently, wish the current price of \$5 for a 3 inch polished wafer or \$1182/kg would reach \$6 to \$6.50 in order to permit a reasonable profit. Using the wished for price, we arrive at prices of \$1418/kg to \$1537/kg which compares reasonably with our estimated cost of \$1393/kg.

The cost of producing polished wafers in space by the float zone process starting with polycrystalline material depends significantly on the cost to transport this material into space.

Using Equation C.1 and choosing the extremes of a range of transportation costs equal to \$100/kg to \$1000/kg, we estimate the cost of producing polished silicon wafers in space as follows:

For T = \$100/kg:

C_{pw} = (10 + 100 + 120) ÷ (0.75 x 0.50 x 0.82 x 0.85) +

175 (0.50 x 0.82 x 0.85) + 0 + 150 ÷ 0.85 = \$1568/kg

For T = \$1000/kg:

C_{pw} = (10 + 1000 + 120) ÷ (0.75 x 0.50 x 0.82 x 0.85) +

175 (0.50 x 0.82 x 0.85) + 0 + 150 ÷ 0.85 = \$5051/kg

It is important to note here that the resultant cost figures estimated for space manufacture of silicon wafers assume that the fixed costs of processing and the yield of each step is the same as that engendered in an Earth process. This assumption implies the labor costs in space and the cost of facility and power in space are the same as on Earth. Such an assumption favors the cost of space processing vis-a-vis Earth processing because labor costs (due transportation and life support) are bound to be greater than those on Earth, the cost of a manufacturing facility in space (due transportation and additional labor costs) must be greater than a comparable facility on Earth and the cost of power produced in space can only hope to equal that produced on Earth. The ratio of the estimated costs to produce polished bare Si wafers in space relative to production on Earth at a future time is, therefore, 1.32 or 4.27, corresponding to assumed values for transportation to low Earth orbit of \$100/kg or \$1000/kg, respectively.

Finally, we estimate the additional costs associated with the final processing of a bare, polished Si wafer into a substrate for an electronic device. Because this final processing, as mentioned in Section C.2, is dominated by handling charges, it is nearly independent of wafer diameter. Therefore, a comparison of added costs, as dependent on wafer size, are best illustrated by an index equal to the cost per final useful area (\$/cm^2). Importantly, the economic potential of space manufacture of devices using a Si substrate depends on the possibility of manufacturing crystals in diameters greater than that possible on Earth. The benefits of this potential arise only in the final processing of a larger polished wafer into a substrate for use in an electronic device.

In the calculation of the cost of a substrate for a variety of useful electronic devices, we transform the cost of a wafer of given diameter to the cost per unit of area as follows:

The mass of a single wafer, $m_w = \frac{\pi d^2}{4} \times t\rho$ (C.3)

where:

m_w = mass of wafer, gm

$\frac{\pi d^2}{4}$ = area of wafer, cm^2

d = diameter of water, cm

t = thickness of wafer, cm

ρ = density of Si = 2.42 gm/cm^3

The cost of a bare, polished wafer per unit area = cost per unit area - cost per unit mass x mass/unit area = $C_{pw} \times t\rho$ (C.4)

The cost of a bare, polished wafer = cost per unit mass x mass of wafer =

$$C_{pw} \times \frac{\pi d^2}{4} \times t\rho \qquad (C.5)$$

Tables C.1 and C.2 below, illustrate the results of conversion of costs, from the \$/kg to the $\$/cm^2$ base, using the cost per unit mass previously developed for Earth and space-based processing. The costs are based on 1976 dollars as indicated.

The additional cost component attributed to the Si substrate in a finished electronic device has two elements. The first cost element involves necessary handling, transfers, inspection and tests. This depends mostly on the complexity of the final device and not on wafer diameter as illustrated in Figure C.2. The cost vs. complexity for a 7.62 cm (3 in.) bare wafer is derived from current practice. The value added to a bare wafer involved in final processing is assumed to be the same for the larger wafer sizes. Another cost increment is due to the yield resulting from the processing of a bare, polished wafer into its final form, most often a chip. Inevitable losses due to handling and cutting to a final form occur. A rim loss due to handling is unavoidable. Also, most often, the final form of the Si substrate is a square chip and cutting these chips from a circular wafer entails unavoidable losses due geometric considerations. Figure C.3 illustrates the yields associated with final processing as dependent on the final form of the substrate used.

We estimate the cost of the Si substrate produced either on Earth or in space for different products by using the formula:

$$C_f = (C_{pw} \times \Delta C_{pw}) \div (Y_f \times A_w) \qquad (C.6)$$

C_f = final cost of Si substrate in finished device, $\$/cm^2$

C_{pw} = cost of bare, polished silicon wafer entering final processing, \$/kg

ΔC_{pw} = incremental value added due to processing wafer to form used in final device, \$/kg

Y_f = yield of processing wafer to final form of substrate

A_w = area of bare, polished wafer, cm^2

Tables C.3, C.4 and C.5 show and compare the cost of a finished Si substrate for solar cells or rectifiers, common metal oxide semiconductors (MOS) or integrated circuits (IC) and bipolar integrated circuits produced on Earth and in space. The results shown in these tables use the data (C_{pw} and A_w) appearing in Tables C.1 and C.2 as a starting point and applies Equation C.6 with values of Y_f from Figure C.3 and values of ΔC_{pw} from Figure C.2*. The values of ΔC_{pw} for either an Earth-based or space-based process are assumed equal.

C.4 SUMMARY IMPACT ANALYSIS

The total market value for bare silicon wafers is now approximately 225 million dollars. It has had a past rate of growth of about 20% per year. If this rate of growth were to continue it would reach 8.6 billion dollars by the year 1995 and in the decade 1995 to 2005 (when space transport costs of $100/kg are predicted), a cumulative ten-year market of 258 billion dollars would obtain. This appears somewhat unlikely, but it might serve as an upper limit. If the rate of growth of the silicon wafer market increased at the average rate of 10% per year, the market in the year 1995 would be 1.5 billion dollars and a cumulative market of approximately 27 billion dollars in the ten year span between 1995 and 2005. Accept, for purposes of illustration, a 30 billion dollar cumulative market for the decade following 1995.

There is almost no economic incentive to produce larger wafers that will not be processed into finished electronic devices (wafers used in power rectifiers are an exception, but have little impact on the total market.) Currently about 60% of bare wafers are processed to finished devices. Assuming this figure remains the same in future years, the potential cumulative market for larger wafers reduces to 18 billion dollars. Of this possible market for Si wafers, those produced by the float zone process can only hope to have its share.

The portion of the current market for Si crystal wafers produced by the float zone method is small relative to those produced by the Czochralski method. Float zone produced wafers get their market share primarily through superior crystal quality, not through any advantage of size or cost.

---

*The incremental value shown in Figure C.2 is estimated to be equal to the difference between the price of the packaged electronic device per unit wafer size minus the cost of the bare wafer of the same size entering the process. The incremental value calculated in this manner overemphasizes the added value attributed to the crystal Si substrate alone.

In addition, there is nothing obviously fallacious in the argument that Si wafers of sizes equal to that possible by the float zone space process can either be grown on Earth or in space by the Czochralski method. Following these arguments, we assume that the market for crystal wafers in the decade 1995 to 2005 will be distributed among final applications in the same manner as now. Moreover, we assume that the market share for float zone crystal, in application to final electronic devices, will be distributed as it is now. Finally, we estimate the potential impact on the U.S. electronics industry of float-zone crystal wafers produced in space by computing the potential savings attendant to each market segment (as described in the SUMMARY) and adding them. Table C.6 below lists the values used in the final estimate of potential savings.

Assuming that the potential cumulative market for finally processed wafers in the decade 1995-2005 is 18 billion dollars, we estimate the total potential savings by multiplying the value by the product of the fractions appearing in each row of Table C.6 and summing them as follows:

$$18 \times 0.17 \times 0.02 \times 0.11 = 0.00673$$
$$18 \times 0.31 \times 0.05 \times 0.45 = 0.12555$$
$$18 \times 0.20 \times 0.03 \times 0.62 = 0.06696$$
$$18 \times 0.32 \times 0.01 \times 0.65 = 0.03744$$

Total = .237 billion dollars
= 237 million dollars

TABLE C.1

ESTIMATED COST OF BARE, POLISHED Si WAFER PRODUCED ON EARTH

Wafer Diameter (cm)	Wafer Diameter (in)	Wafer Thickness (cm)	Mass/unit area (gm/cm^2)	Area (cm^2)	Mass (gm)	Cost per Unit Wafer: Wafer ($)	Cost per Unit Wafer: Area ($/cm^2$)
7.62	3	.04	0.097	45.6	4.23	5.0	0.115
15.2	6	.08	0.194	182.3	35.0	41.3	0.229
30.5	12	.14	0.339	729.3	247.0	292.0	0.401

1) Polished bare wafer cost = $1182/kg
2) Polycrystalline cost = $10/kg
3) 1976 dollars

TABLE C.2

ESTIMATED COST OF BARE, POLISHED Si WAFER PRODUCED IN SPACE

Wafer Diameter (cm)	Wafer Diameter (in)	Cost: Transportation Cost $100/kg: Wafer ($)	Cost: Transportation Cost $100/kg: Per Unit Wafer Area ($/cm^2)	Cost: Transportation Cost $1000/kg: Wafer ($)	Cost: Transportation Cost $1000/kg: Per Unit Wafer Area ($/cm^2)
7.62	3	6.93	0.152	22.3	0.490
15.2	6	55.4	0.304	178.6	0.980
30.5	12	387.7	0.532	1248.6	1.712

1) Polished bare wafer cost = $1568/kg
   @ transportation cost = $ 100/kg
2) Polished bare wafer cost = $5051/kg
   @ transportation cost = $1000/kg
3) Polycrystalline cost = $ 10/kg
4) 1976 dollars

TABLE C.3

ESTIMATED COST OF FINISHED Si SUBSTRATE FOR SOLAR CELL OR RECTIFIER

	Earth Process			Space Process					
Transportation Cost ($/kg)	0			100			$1000		
Wafer diameter (cm)	7.62	15.2	30.5	7.62	15.2	30.5	7.62	15.2	30.5
Wafer diameter (in)	3	6	12	3	6	12	3	6	12
Cost of bare wafer ($)	5.0	41.3	292.0	6.9	55:4	387.7	22.3	178.6	1248.6
Incremental cost of finishing ($)	13.0	13.0	13.0	13.0	13.0	13.0	13.0	13.0	13.0
Cost of finished wafer ($)	18.0	64.3	305.0	19.9	68.4	400.7	35.3	191.6	1261.6
Yield (wafer to final product)* (%)	84	92	95	84	92	95	84	92	95
Substrate cost ($)	21.4	69.9	321.1	23.7	74.3	421.8	42.0	208.3	1328.0
Si substrate Cost ($/cm^2)	.469	.383	.440	.519	.408	.578	.92	1.14	1.82

*Final product in wafer form with rim trim only

TABLE C.4

ESTIMATED COST OF FINISHED Si SUBSTRATE FOR MOS OR IC

	Earth Process			Space Process					
Transportation Cost ($/kg)	0			100			1000		
Wafer diameter (cm)	7.62	15.2	30.5	7.62	15.2	30.5	7.62	15.2	30.5
Wafer diameter (in)	3	5	12	3	6	12	7	6	12
Cost of bare wafer ($)	5.0	41.3	292.0	6.9	55.4	387.7	22.3	178.6	1248.6
Incremental cost of finishing ($)	38.0	38.0	38.0	38.0	38.0	38.0	38.0	38.0	38.0
Cost of finished wafer ($)	43.0	79.3	230.0	44.9	93.4	425.7	60.3	216.6	1268.6
Yield (wafer to final product * (%)	72	80	90	72	80	90	72	80	90
Si substrate cost ($)	59.7	99.1	255.6	62.4	116.8	473.0	83.8	270.8	1409.6
Si substrate cost ($/cm^2)	1.31	0.54	0.35	1.36	0.64	0.65	1.89	1.49	1.93

* For 0.36 cm (0.14 in) square chip

TABLE C.5

ESTIMATED COST OF FINISHED Si SUBSTRATE FOR BIPOLAR IC

	Earth Process			Space Process					
Transportation Cost ($/kg)	0			100			1000		
Wafer diameter (cm)	7.62	15.2	30.5	7.62	15.2	30.5	7.62	15.2	30.5
Wafer diameter (in)	3	6	12	3	6	12	3	6	12
Cost of bare wafer ($)	5.0	41.3	292.0	6.9	55.4	387.7	22.3	178.6	1248.6
Incremental cost of finishing ($)	57.0	57.0	57.0	57.0	57.0	57.0	57.0	57.0	57.0
Cost of finished wafer ($)	62.0	98.3	349.0	63.9	112.4	444.7	79.3	235.6	1305.6
Yield (wafer to final product * (%)	73	81	91	73	81	91	73	81	91
Si substrate cost ($)	84.9	121.4	383.5	87.5	138.8	488.7	108.6	290.9	1434.7
Si substrate cost ($/cm^2)	1.86	0.67	0.53	1.92	0.76	0.67	2.38	1.60	1.97

* For 0.25 cm (0.10 in) square chip

TABLE C.6

ESTIMATED ECONOMIC IMPACT OF SPACE-BASED PRODUCTION OF Si WAFERS BY THE FLOAT-ZONE PROCESS

Market Segment	Percent of Total Market (%)	Float-zone Share (%)	Potential Savings (fraction)
Solar Cell, Si Diode, Rectifier	17	2	.11
Transistor, Thyristor	31	5	.45
MOS, IC	20	3	.62
Bipolar IC	32	1	.65

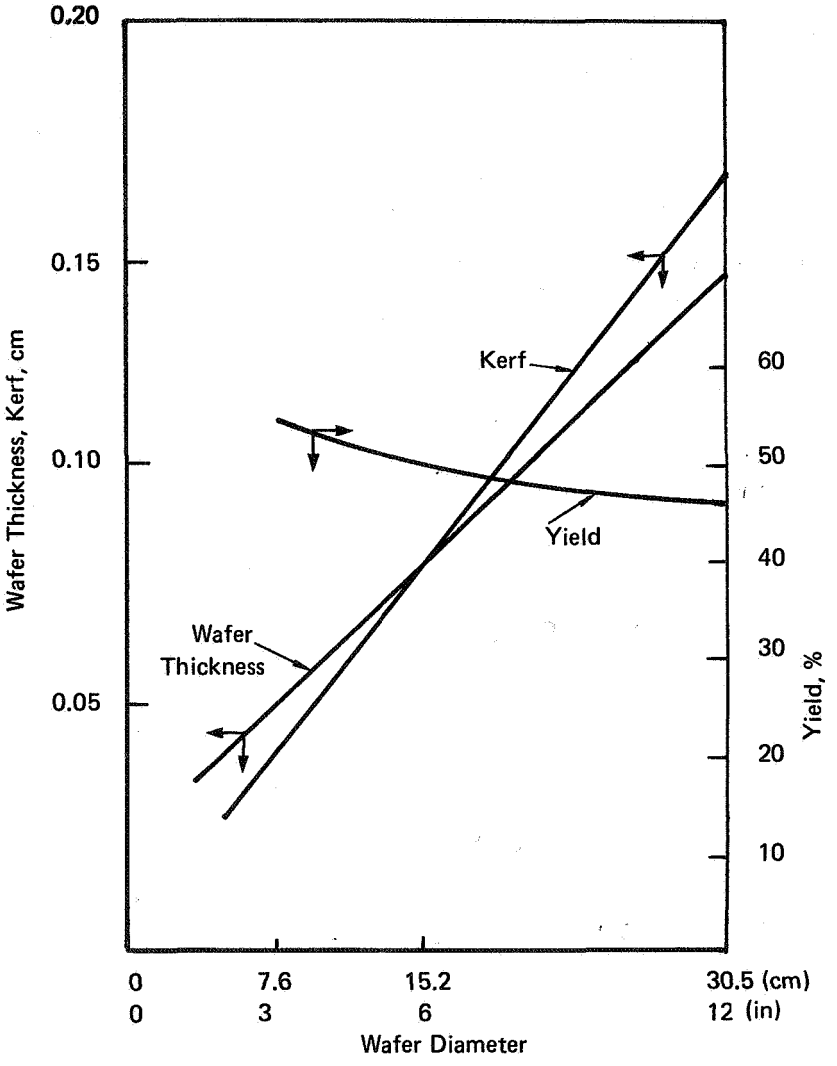

FIGURE C.1 ESTIMATED YIELD OF SAWING PROCESS – FROM TRIMMED BOULE TO WAFER

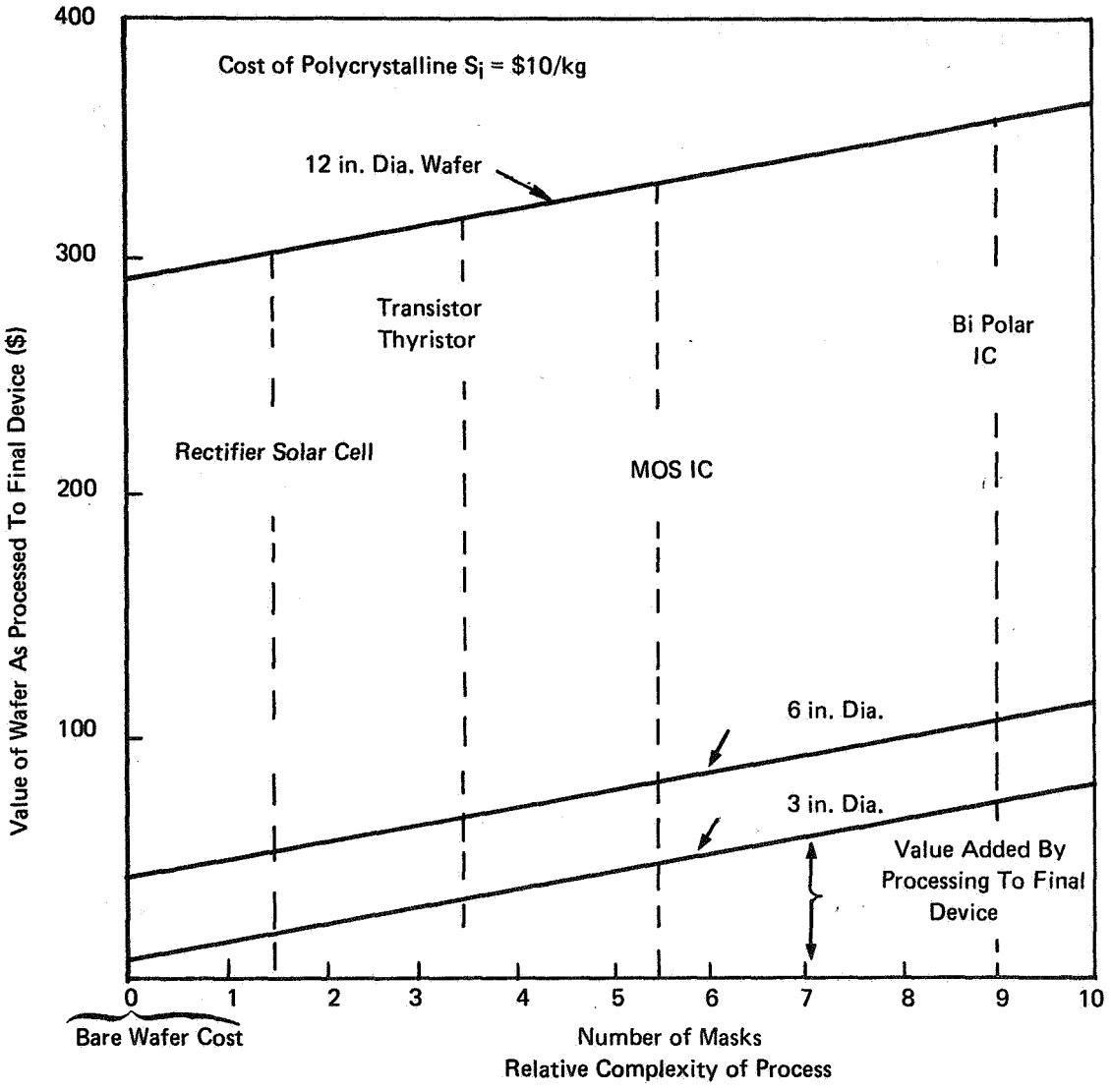

FIGURE C.2 ESTIMATED VALUE OF EARTH FLOAT ZONE PROCESSED WAFERS VS. COMPLEXITY OF FINAL APPLICATION

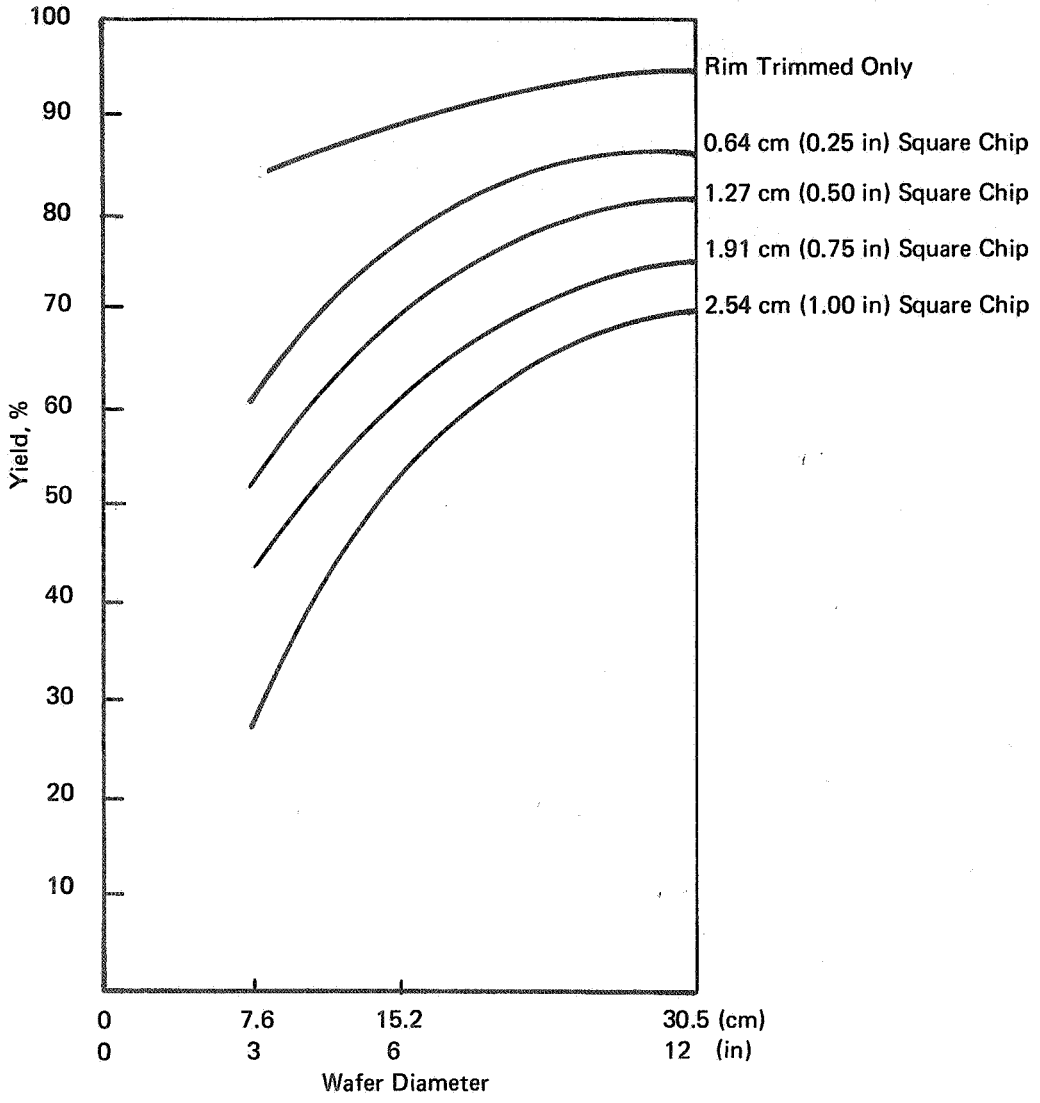

FIGURE C.3 ESTIMATED YIELD IN POLISHED WAFER TO CHIP PROCESS

APPENDIX D

1. Arthur D. Little, Inc., Float Zone Processing in a Weightless Environment, Interim Report to NASA, G. C. Marshall Space Flight Center, NAS8-29877, October 1974

2. Chang, C. E. and Wilcox, W. R., Analysis of Surface Tension Driven Flow in Floating Zone Melting, Int. J. Heat and Mass Transfer, Vol. 19, pp 355-366, April 1976.

3. Hocking, L. M. The Stability of a Rigidly Rotating Column of Liquid, Mathematika, Vol. 7, Part 1, June 1960.

4. NASA Skylab Demonstration Films (16mm), Stock No. 6750-0000001, (1) TV101-012, SL4-485; (2) TV101-013, SL4-486; (3) TV101-014-1, SL4-492; (4) TV101-014-2, SL4-493; (5) TV101-016, SL4-494.

5. Altman, J. H., F. Grum and Nelson, C.N.,Photographic Speeds Based on Radiant Energy Units. Photographic Science & Engineering Vol. 17, No. 6, November/December 1973.

6. Lamb, Sir H., Hydrodynamics, 6th Ed., New York, Dover Publication, 1945, P. 597.

NATIONAL AERONAUTICS AND SPACE ADMINISTRATION
WASHINGTON, D.C. 20546

OFFICIAL BUSINESS
PENALTY FOR PRIVATE USE $300

SPECIAL FOURTH-CLASS RATE
BOOK

POSTAGE AND FEES PAID
NATIONAL AERONAUTICS AND
SPACE ADMINISTRATION
451

U.S.MAIL

POSTMASTER: If Undeliverable (Section 158
Postal Manual) Do Not Return

"The aeronautical and space activities of the United States shall be conducted so as to contribute . . . to the expansion of human knowledge of phenomena in the atmosphere and space. The Administration shall provide for the widest practicable and appropriate dissemination of information concerning its activities and the results thereof."

—NATIONAL AERONAUTICS AND SPACE ACT OF 1958

NASA SCIENTIFIC AND TECHNICAL PUBLICATIONS

TECHNICAL REPORTS: Scientific and technical information considered important, complete, and a lasting contribution to existing knowledge.

TECHNICAL NOTES: Information less broad in scope but nevertheless of importance as a contribution to existing knowledge.

TECHNICAL MEMORANDUMS: Information receiving limited distribution because of preliminary data, security classification, or other reasons. Also includes conference proceedings with either limited or unlimited distribution.

CONTRACTOR REPORTS: Scientific and technical information generated under a NASA contract or grant and considered an important contribution to existing knowledge.

TECHNICAL TRANSLATIONS: Information published in a foreign language considered to merit NASA distribution in English.

SPECIAL PUBLICATIONS: Information derived from or of value to NASA activities. Publications include final reports of major projects, monographs, data compilations, handbooks, sourcebooks, and special bibliographies.

TECHNOLOGY UTILIZATION PUBLICATIONS: Information on technology used by NASA that may be of particular interest in commercial and other non-aerospace applications. Publications include Tech Briefs, Technology Utilization Reports and Technology Surveys.

Details on the availability of these publications may be obtained from:

SCIENTIFIC AND TECHNICAL INFORMATION OFFICE

NATIONAL AERONAUTICS AND SPACE ADMINISTRATION

Washington, D.C. 20546